Gondwana Research 67 (2019) 82–100

Contents lists available at ScienceDirect

Gondwana Research

journal homepage: www.elsevier.com/locate/gr

The shutdown of an anoxic giant: Magnetostratigraphic dating of the end of the Maikop Sea

D.V. Palcu [a,*], S.V. Popov [b], L.A. Golovina [c], K.F. Kuiper [d], S. Liu [a,e], W. Krijgsman [a]

[a] Paleomagnetic Laboratory 'Fort Hoofddijk', Utrecht University, Budapestlaan 17, 3584 CD Utrecht, the Netherlands
[b] Borissiak Paleontological Institute, Russian Academy of Sciences, Profsoyuznaya ul., 123, Moscow 117997, Russia
[c] Geological Institute, Russian Academy of Sciences, Pyzhevskiy per. 7, Moscow 119017, Russia
[d] Department of Sciences, Vrije Universiteit, Amsterdam 1081-HV, the Netherlands
[e] State Key Laboratory of Lithospheric Evolution, Institute of Geology and Geophysics, Chinese Academy of Sciences, Beijing 100029, China

ARTICLE INFO

Article history:
Received 19 March 2018
Received in revised form 29 September 2018
Accepted 30 September 2018
Available online 4 December 2018

Handling Editor: N. Rawlinson

Keywords:
Anoxia
Paratethys
Maikop
Middle Miocene
Biostratigraphy
Magnetostratigraphy
Marine flooding
Paleogeography
Tarkhanian
Chokrakian
Karaganian
Marine gateways
Tectonic-eustatic interplay

ABSTRACT

Paratethys, the lost sea of central Eurasia, was an anoxic giant during Oligocene – early Miocene (Maikop Series) times. With a size matching the modern-day Mediterranean Sea and a history of anoxic conditions that lasted for over 20 Myrs, the eastern part of this realm (Black Sea-Caspian Sea domain) holds key records for understanding the build-up, maintenance and collapse of anoxia in marginal seas. Here, we show that the collapse of anoxic Maikop conditions was caused by middle Miocene paleogeographic changes in the Paratethys gateway configuration, when a mid-Langhian (Badenian-Tarkhanian) transgression flooded and oxygenated the Eastern Paratethys. We present an integrated magneto-biostratigraphic framework for the early Middle Miocene (Tarkhanian-Chokrakian-Karaganian regional stages) of the Eastern Paratethys and date the lithological transition from anoxic black shales of the Maikop Series to fossiliferous marine marls and limestones of the regional Tarkhanian stage. For this purpose, we selected two long and time-equivalent sedimentary successions, exposed along the Belaya and the Pshekha rivers, in the Maikop type area in Ciscaucasia (southern Russia). We show that a significant but short marine incursion took place during the Tarkhanian, ending the long-lasting Maikop anoxia of the basin. Our magnetostratigraphic results reveal coherent polarity patterns, which allow a straightforward correlation with the time interval 15–12 Ma of the Geomagnetic Polarity Time Scale. The Tarkhanian flooding occurred during a relatively short normal polarity interval that correlates with C5Bn, resulting in an age of 14.85 Ma. The regional Tarkhanian/Chokrakian stage boundary is located within C5ADn at an age of 14.75 Ma and the Chokrakian/Karaganian boundary is tentatively correlated with C5ACn and an age of 13.9–13.8 Ma. Our new Tarkhanian flooding age reveals a paleogeographic scenario that is different from many previous reconstructions. Instead of envisaging marine connections to the Indian Ocean, we show that major changes in connectivity between the Eastern and Central Paratethys seas have caused the influx of marine waters during the Tarkhanian. An increase in marine connectivity with the Mediterranean during a short episode of rapid sea-level rise triggered mixing and ended the widespread anoxia in the Eastern Paratethys. The mixing episode was short-lived (~100 kyr) as the sea-level rise slowed down and connectivity degraded because of tectonic uplift in the gateway area.

1. Introduction

The Eocene Peri-Tethys sea gradually transformed into the Paratethys (Laskarev, 1924) during the latest Eocene-early Oligocene as a result of tectonic processes in the Eurasia-Afro/Arabia collision zone (e.g. Schultz et al., 2005; Van der Boon et al., 2018). The open marine Peri-Tethys mainly governed widespread deposition of whitish marls and limestones in central Eurasia, but the highly restricted Paratethys domain predominantly shows dark, organic-rich shales. The anatomy of the Paratethys realm is relatively simple: it consists of numerous (sub) basins, characterized by restricted connectivity and poorly oxygenated environments, that are surrounded by fresh to brackish water lake systems (Figs. 1, 2). Salinity stratification and the lack of vertical circulation led to the formation of anoxic waters, which especially remained tethered in the deep depressions of the Euxinic (Black Sea) and Caspian basins. Shallower basins, with limited anoxia, bordered the deeper basins and recorded mixed influences from seas and rivers that drained a large surface of central Eurasia. Shallow seaways and straits provided restricted exchange with the global ocean and probably encouraged stratification of the water column.

* Corresponding author.
E-mail address: d.v.palcu@uu.nl (D.V. Palcu).

https://doi.org/10.1016/j.gr.2018.09.011
1342-937X/

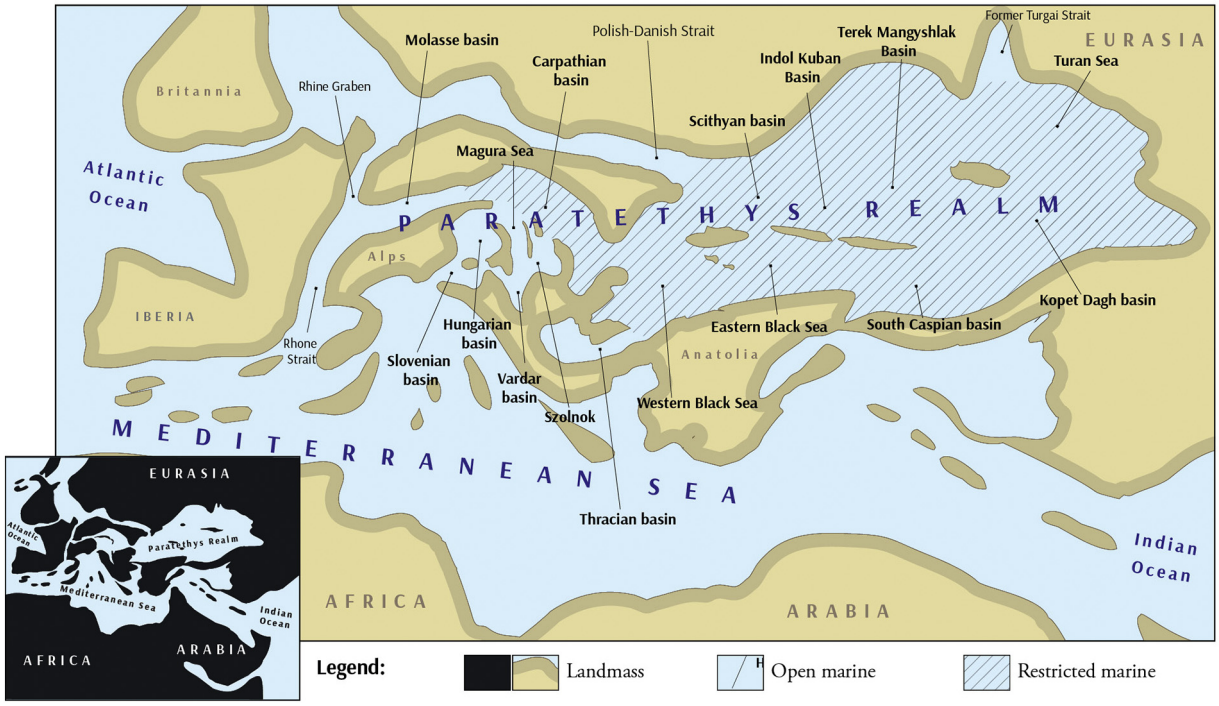

Fig. 1. The seas of the Paratethys realm at their maximum extent during the Lower Oligocene (35–30 Ma) (Popov et al., 2004) and their paleoenvironments: anoxic basins - Eastern Paratethys, Carpathian basin; restricted marine basins - Alpine Molasse basin, Hungarian basin, Vardar basin; marine seaways - Polish-Danish strait, Rhine Graben, Rhone strait.

During Oligo-Miocene times, organic-rich anoxic shales of the Maikop Sea (with TOC values up to 14%: Robinson et al., 1996; Katz et al., 2000) were deposited in the Eastern Paratethys domain. This domain was gigantic in size, with a surface of ~1.8 × 10^6 km^2 (75% the size of the present-day Mediterranean) and volume of ~16 × 10^6 km^3, containing 80% of the total Paratethys waters (estimation based on the paleogeographic data of Popov et al., 2006). This anoxic giant provides the main hydrocarbon source rocks for the Black Sea and South Caspian basins, where the Maikop Series reaches a maximum thickness of ~1000 and ~2000 m, respectively. The total organic sedimentary carbon stored in the Maikop Series and its equivalents was estimated at 60 × 10^{12} T, which may have significantly contributed to suppressed atmospheric CO_2 levels throughout the Oligocene (Allen and Armstrong, 2008).

In this paper we construct a new chronological framework for the sedimentary successions of the Eastern Paratethys by applying integrated magneto-biostratigraphic and radio-isotopic dating techniques to the uppermost Maikopian-Tarkhanian-Chokrakian successions exposed along the Belaya and Pshekha rivers (Fig. 4). Our new age model will allow to date the end of anoxic conditions in the Eastern Paratethys, to correlate the stratigraphy of the Eastern Paratethys with the Central Paratethys successions and to clarify the relationship between the two realms in various eustatic settings. The results will be discussed from the perspective of eustatic and tectonic forcing in the gateways and will provide a new scenario for the connectivity history between the two Paratethys domains and the open ocean.

2. Geological and stratigraphic background

Throughout the Oligocene, the tectonic built-up of the Alpine-Balkan-Pontides-Alborz-Kopet Dag orogenic belt has progressively isolated the intercontinental Paratethys Sea from the Mediterranean basin (e.g. Rögl, 1998; Popov et al., 2004). At its peak development (Fig. 1), Paratethys stretched on longitude from Switzerland to Turkmenistan and on latitude from the south Urals to Anatolia. Paratethys was generally connected to the global ocean via shallow and narrow gateways; the Rhone Strait, Rhine Graben, Polish-Danish Strait and potentially the Araks Strait through Iran (Fig. 2C). It encompassed deep anoxic basins like the Carpathian foredeep, Indol-Kuban basin, Terek-Mangyshlak, Fore-Kopet Dag, Black Sea and the South Caspian Basin, shallower seas with occasional anoxia on the Scythian and Turan shelfs, and seas that are relatively well connected to the global ocean as the Alpine Molasse basin, the Hungarian basin, Thracian basin, Magura Sea, Szolnok Trough and the Slovenian basin.

During the Early Miocene (Fig. 2A), Paratethys covered the area from the Vienna Basin in Austria to the western Kopet Dag in Turkmenistan (Popov et al., 2006). At this time, Paratethys was fragmented in smaller sub-basins that were grouped in two systems: The Central European (Central Paratethys) and the Euxinian-Caspian (Eastern Paratethys). The Central Paratethys consisted in a western branch, the Karpatian Sea, that was connected to the Mediterranean realm (Brzobohathy et al., 2003; Kováč et al., 2007; Sant et al., 2017) and an eastern branch, to which we refer as the Grey Sea (Palcu et al., 2017), characterized by low salinity and restricted connectivity both to the west and east (Fig. 2A). The Eastern Paratethys extended from Bulgaria and Romania to the Kopet Dag in Turkmenistan, Central Asia (Fig. 2A). As a result, regional stratigraphic stages have been defined for both the Central and the Eastern Paratethys (e.g. Nevesskaya et al., 2005b; Piller et al., 2007; Hilgen et al., 2012).

Barbot de Marny (1869) and Andrusov (1917) initiated the construction of a regional stratigraphic scale for the Eastern Paratethys, which has later been transformed into officially defined regional stages (6th Congress on Regional Neogene Stratigraphy - RCMNS, 4-7 September 1975). The proposed stratotypes were located in shallow basins, rich in mollusk assemblages (the main stratigraphic group in Andrusov's time) but commonly dealt with incomplete successions. These stratotypes have been excellent for describing the faunas corresponding to each of the regional stages but they were not suitable for the integration of new dating methods that are required to better understand the paleoenvironmental and paleoecological changes in the region. Complete successions comprising Early-Middle Miocene stages of Eastern Paratethys are mainly found in deep water settings

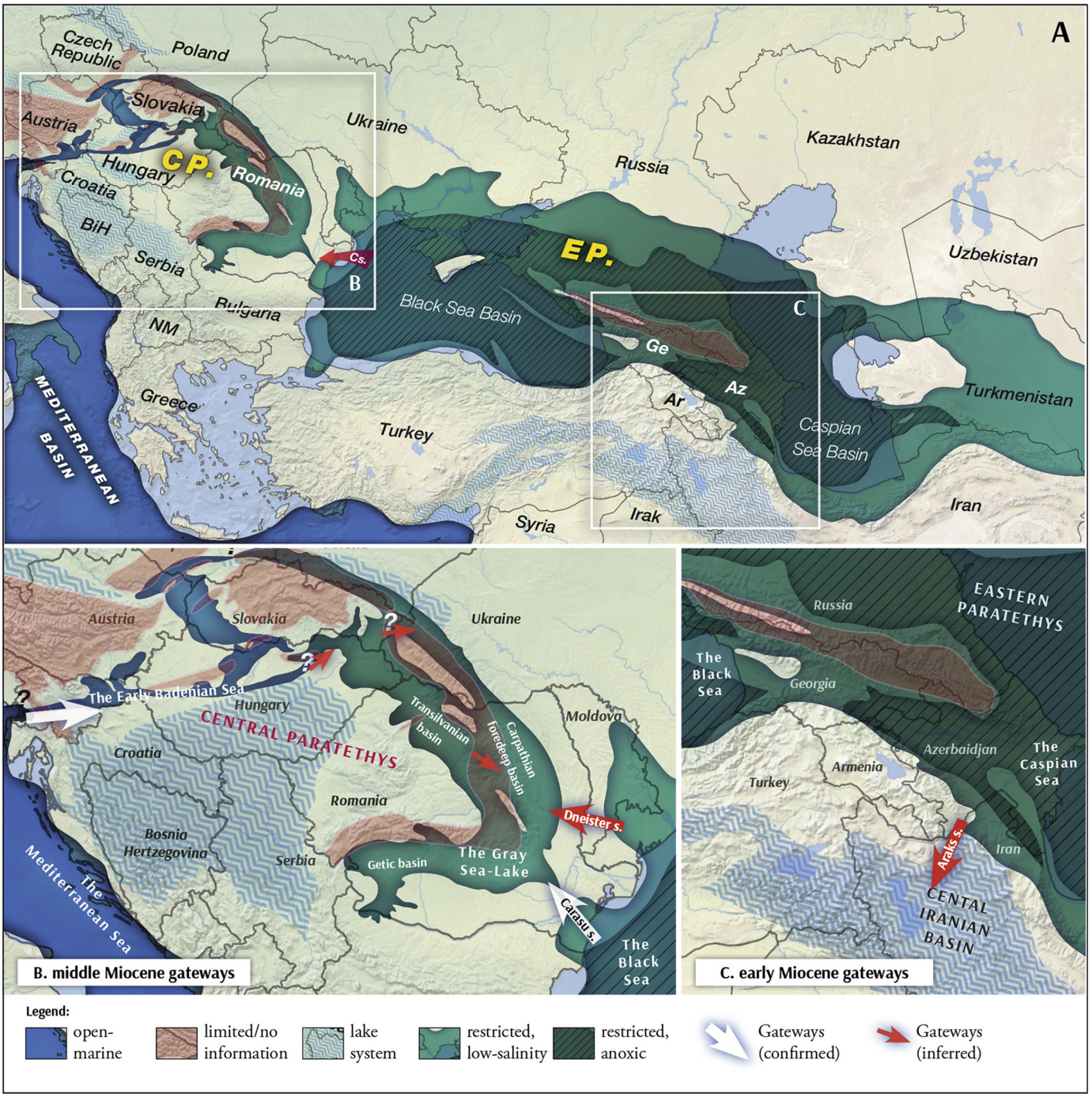

Fig. 2. Paleogeographic setting during the early Miocene (Kozakhurian), before the Badenian/Tarkhanian flooding with focus on the main sea-straits zones.

that are poor in macro-fossils but do contain richer assemblages of planktonic and benthic foraminifera and calcareous nannoplankton (Popov et al., 2015).

The onset of anoxia in the Eastern Paratethys is apparently diachronous, dated as late Eocene (~37.7 Ma) in the Talysh area of Azerbaijan (Van der Boon et al., 2017), at the Eocene-Oligocene boundary (~33.9 Ma) in the Maikop type area (Sachsenhofer et al., 2017) and as earliest Oligocene (~33.7 Ma) in the northeastern Caucasus (Gavrilov, 2017). The end of anoxia in the Eastern Paratethys is generally considered a synchronous event, triggered by a marine transgression that took place at the base of the Tarkhanian regional stage. Two different age models prevail for the Tarkhanian stage (Fig. 3): 1) its base is correlated to the base of the Langhian/Badenian at ~16 Ma (Piller et al., 2007; Hilgen et al., 2012) and 2) it is correlated to the nannoplankton zone NN5 at an age of ~15 Ma (Krasheninnikov et al., 2003; Golovina, 2012; Andreyeva-Grigorovich and Savytskaya, 2000).

Fragmentation and isolation of Eastern Paratethys sections/sediments hampered straightforward correlations to the Geological Time Scale and led to the establishment of the regional Kozakhurian, Tarkhanian, Chokrakian and Karaganian stages (Fig. 3). A reliable time frame for the deep basinal Paratethyan successions is critical to understand the relationship between the geodynamic, eustatic and climatic forcing factors. It will also help to identify paleoenvironmental changes and clarify the water exchange mechanisms and gateway dynamics. During the last decade, significant progress has been made to date the Eastern Paratethys successions by radio-isotope dating and magneto-

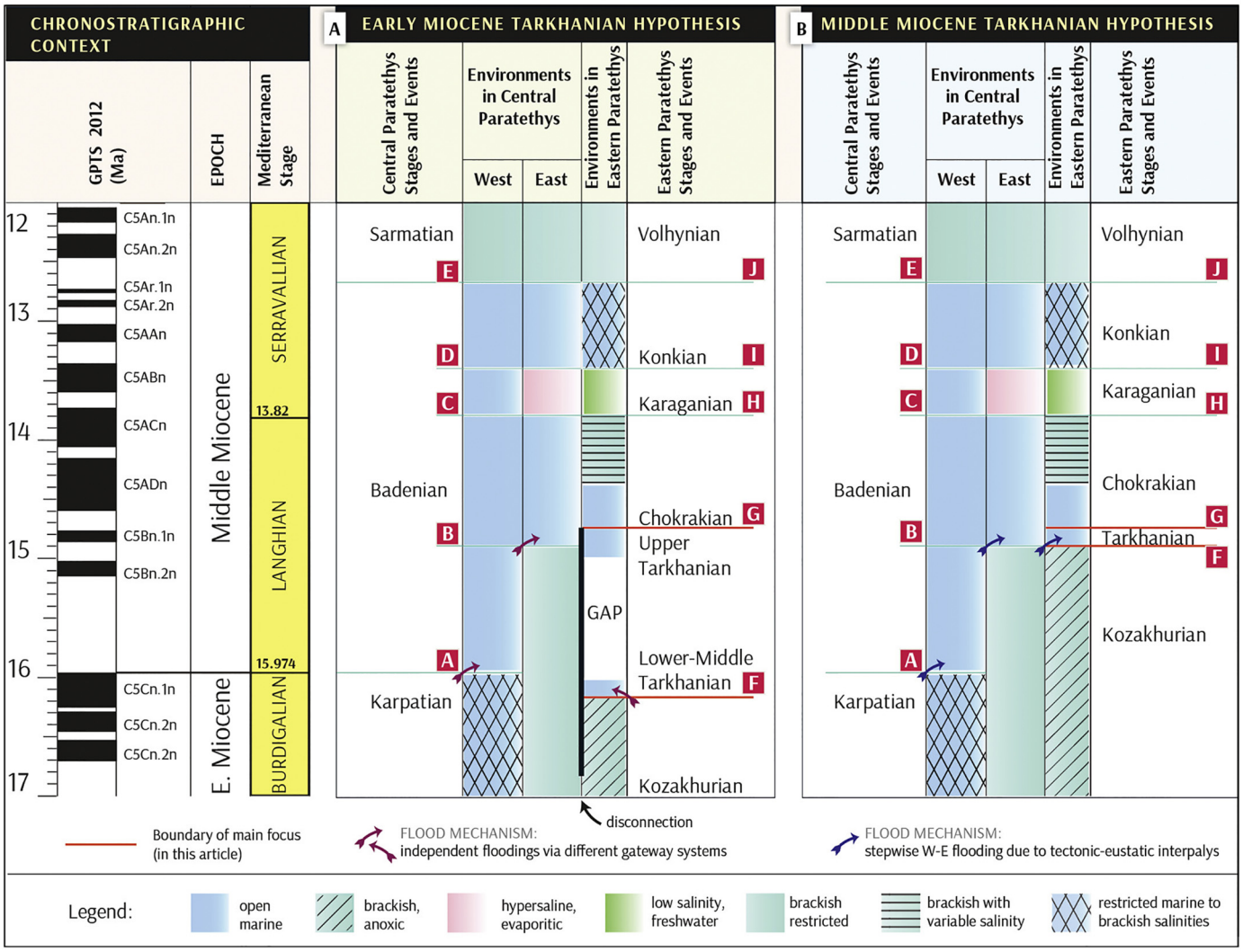

Fig. 3. Middle Miocene stratigraphy of the Mediterranean, Central Paratethys and the two hypotheses of Eastern Paratethys stratigraphy (Hilgen et al., 2012; Palcu et al., 2015; Palcu et al., 2017), paleoenvironments and the main events: (A. The First Badenian flooding in the western half of Central Paratethys, B. Badenian flooding, C. Wieliczian sea-level regression/isolation, D. Upper Badenian flooding, E. Badenian-Sarmatian Extinction Event BSEE, F. Tarkhanian flooding, G. Chokrakian restriction, H. Karaganian isolation, I. Konkian reconnection, J. Konkian - Lower Sarmatian s.l. (Volhynian) extinction).

bio-stratigraphy (e.g. Vangengeim et al., 2006; Vangengeim and Tesakov, 2008; Krijgsman et al., 2010; Vasiliev et al., 2011; Radionova and Golovina, 2012; *Paleontology and stratigraphy of the Middle–Upper Miocene of Taman Peninsula. Part 1. Description of key-sections and benthic fossil groups*, 2016; Palcu et al., 2017, 2018; Van der Boon et al., 2017) allowing correlations to the open ocean zonation, climate and sea level records. The current stratigraphic framework for the Early-Middle Miocene of the Eastern Paratethys is mostly relying on correlations with transgressive-regressive cycles and characteristic faunal assemblages reflecting changes in the hydrological regime of this semi-enclosed basin (Nevesskaya et al., 2005a; Popov et al., 2006). Radio-isotope and magnetostratigraphic age constraints for this time interval are progressively being developed (Palcu et al., 2017).

The uppermost stage of the Maikop Series is called **Kozakhurian**, also referred to as Kotsakhurian (Davitashvili, 1933). It is characterized by brackish-water fauna although very rare euryhaline marine species have also been described. The Kozakhurian strata do not contain any age diagnostic fauna elements. The low faunal diversity suggests a very restricted or even partly isolated position from the open ocean. Based on the presence of common endemic species and genera, faunal exchange between the Kozakhurian basin and the brackish-water upper Ottnangian (Burdigalian) domain of the Central Paratethys have been envisaged, probably through an intermittently open gateway (Popov and Voronina, 1983; Popov et al., 1993).

The Tarkhanian (Andrusov, 1918) contains deposits with marine mollusk associations in shallow facies and marine foraminiferal assemblages, including planktonic forms, in deeper facies. The precise age of the Tarkhanian is still problematic due to the lack of zonal species in the planktonic foraminiferal assemblages. The early Tarkhanian was marked by the onset of a prolonged faunal exchange between the Eastern Paratethys, Central Paratethys and the open ocean. Connections to the Indian Ocean (Fig. 2C) have been suggested via the Middle Araks and/or Aleppo-Urfin straits, and the Central Iranian basin – (Goncharova and Il'ina, 1997; Rögl, 1998; Goncharova et al., 2001). Alternatively, two gateways to the Central Paratethys (Fig. 2B) have been proposed: one via the Dniester strait and the other through the Carasu strait (Chiriac, 1970, Goncharova, 1989, Goncharova et al., 2001).

The Chokrakian, also referred to as Tschokrakian, (Andrusov, 1884) contains deposits with impoverished marine fauna that are more endemic than the Tarkhanian ones. Planktonic biota was dominated by pteropods (*Limacina*) and nektonic organisms, represented by diverse fishes. Salinity in the Chokrakian basin was estimated at ~18–25‰, based on bivalve and gastropod assemblages (Goncharova, 1989; Guzhov, 2017). The Chokrakian basin was most likely connected to

the Carpathian foredeep region in the west through the small and shallow "Carasu Strait" in the southern Dobrogea region of Romania (Palcu et al., 2017). Sediment distribution patterns indicate a transgression during Chokrakian times (Nevesskaya et al., 2003) when the basin expanded especially northward and eastward (Goncharova et al., 2001). Significant parts of the Chokrakian basin comprised shallow shoal zones, favoring an increase in benthic organisms (mollusks, bryozoans, foraminifera, ostracods) and algal-bryozoan bioherms (Nevesskaya et al., 2003). The loss of connectivity is best expressed in the upper Chokrakian, where the diversity of mollusks has sharply decreased, gastropods are often represented by embryonic specimens only (Goncharova, 1989) and benthic foraminifera are generally represented by dwarfed or aberrant specimens (Nevesskaya et al., 2003).

The base of the **Karaganian** (Andrusov, 1917) corresponds to a significant change in Eastern Paratethyan mollusk, foraminifera, and nannoplankton faunas, all indicating a trend towards semi-marine conditions with unstable salinity (e.g. Palcu et al., 2017). Paleogeographically, the Chokrakian-Karaganian transition is interpreted as a change from a semi-closed Chokrakian sea towards an even more restricted (fresher water) sea-lake during the Karaganian (Peryt et al., 2004), indicating that Eastern Paratethys became progressively isolated again from the open ocean. The isolation event is suggested to be caused by the global sea level drop Mi-3b, which indicates that the Karaganian is roughly coeval with the Badenian Salinity Crisis of the Central Paratethys (Peryt et al., 2004; De Leeuw et al., 2010; Palcu et al., 2017).

3. Sections and sampling (litho- and biostratigraphy)

Recently, the Karaganian, Konkian and the Volhynian sub-stage (corresponding to the lower part of Sarmatian s.l.) were dated magneto-bio-stratigraphically in the deep basinal successions of the Taman Peninsula of the NE Black Sea coast (Palcu et al., 2017). In this

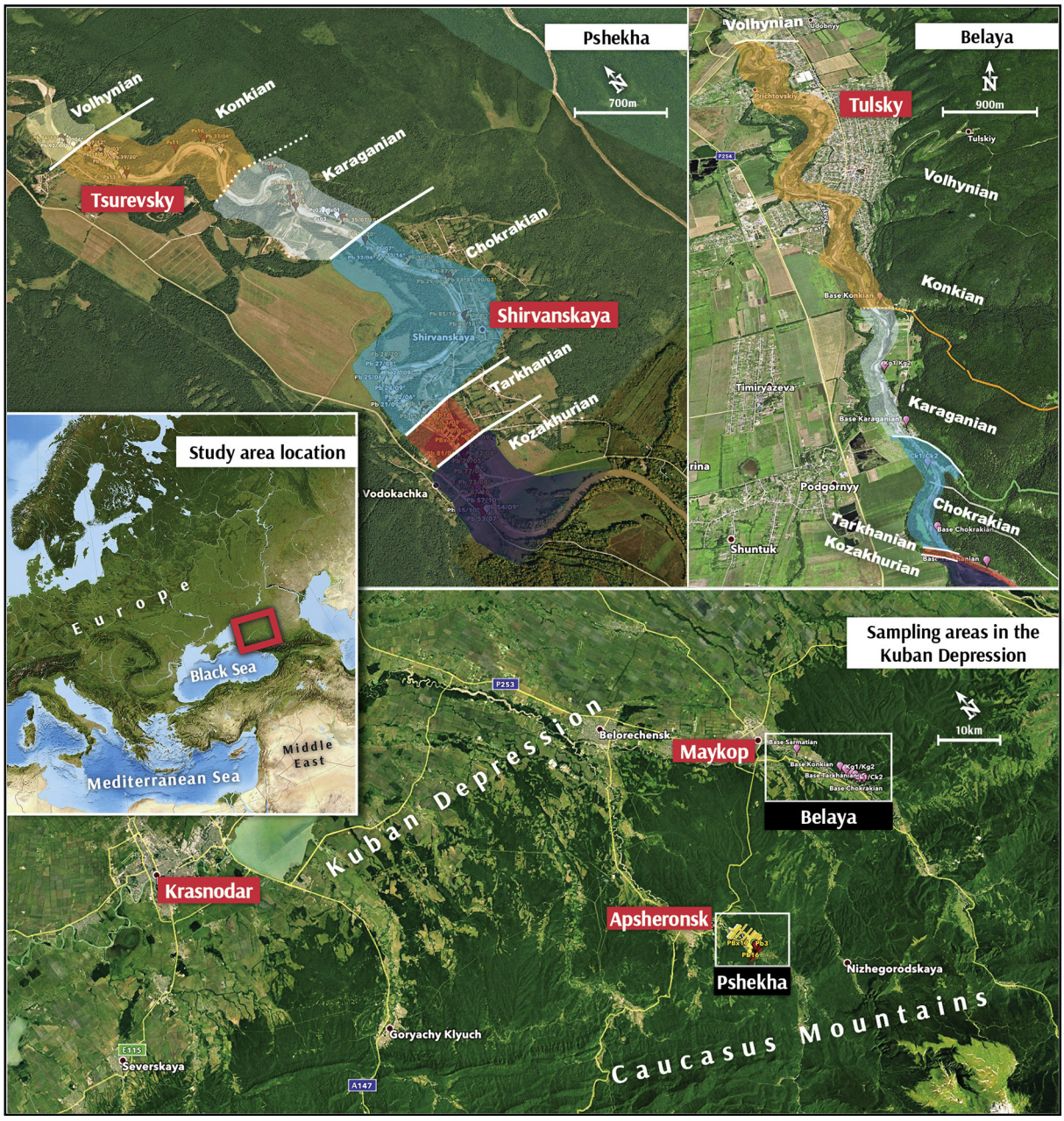

Fig. 4. The location of the Belaya and Pshekha river sections. The color overlays mark the distribution of the stratigraphic units and the respective boundaries between them.

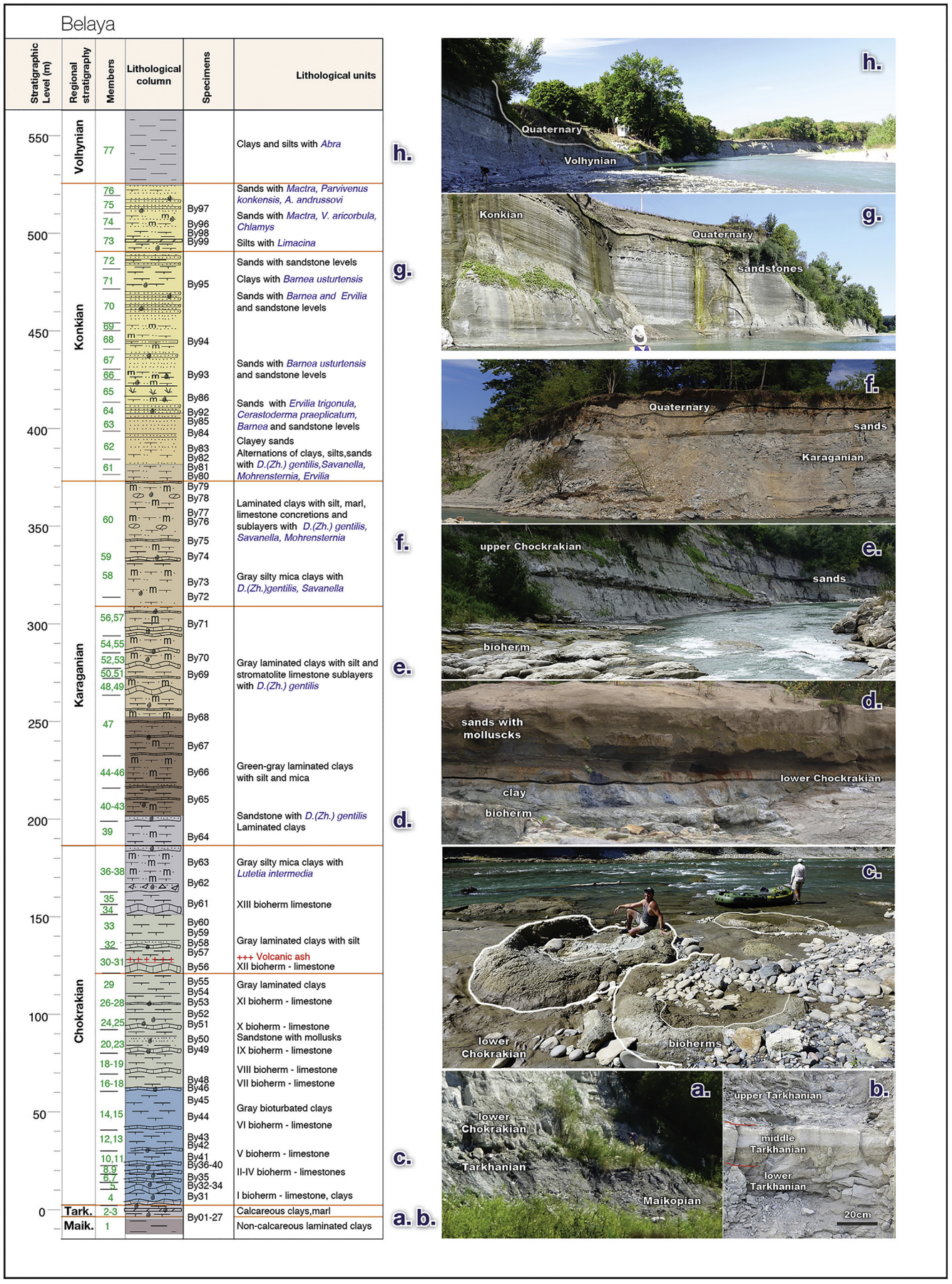

Fig. 5. Bio-lithostratigraphic overview of the Belaya river section.

paper, we focus on determining the ages for the Kozakhurian, Tarkhanian and Chokrakian stages based on sections in Ciscaucasia (northwestern Caucasus; southern Russia). The key-sections are located on the southern margin of the Indol-Kuban basin, in the present-day Krasnodar district (Fig. 4), outcropping along the Belaya and Pshekha rivers. The Belaya and Pshekha sections preserve rather complete successions of deep clayey facies with algal bioherms (Figs. 5, 6), and compose an almost continuous succession from the middle Eocene to

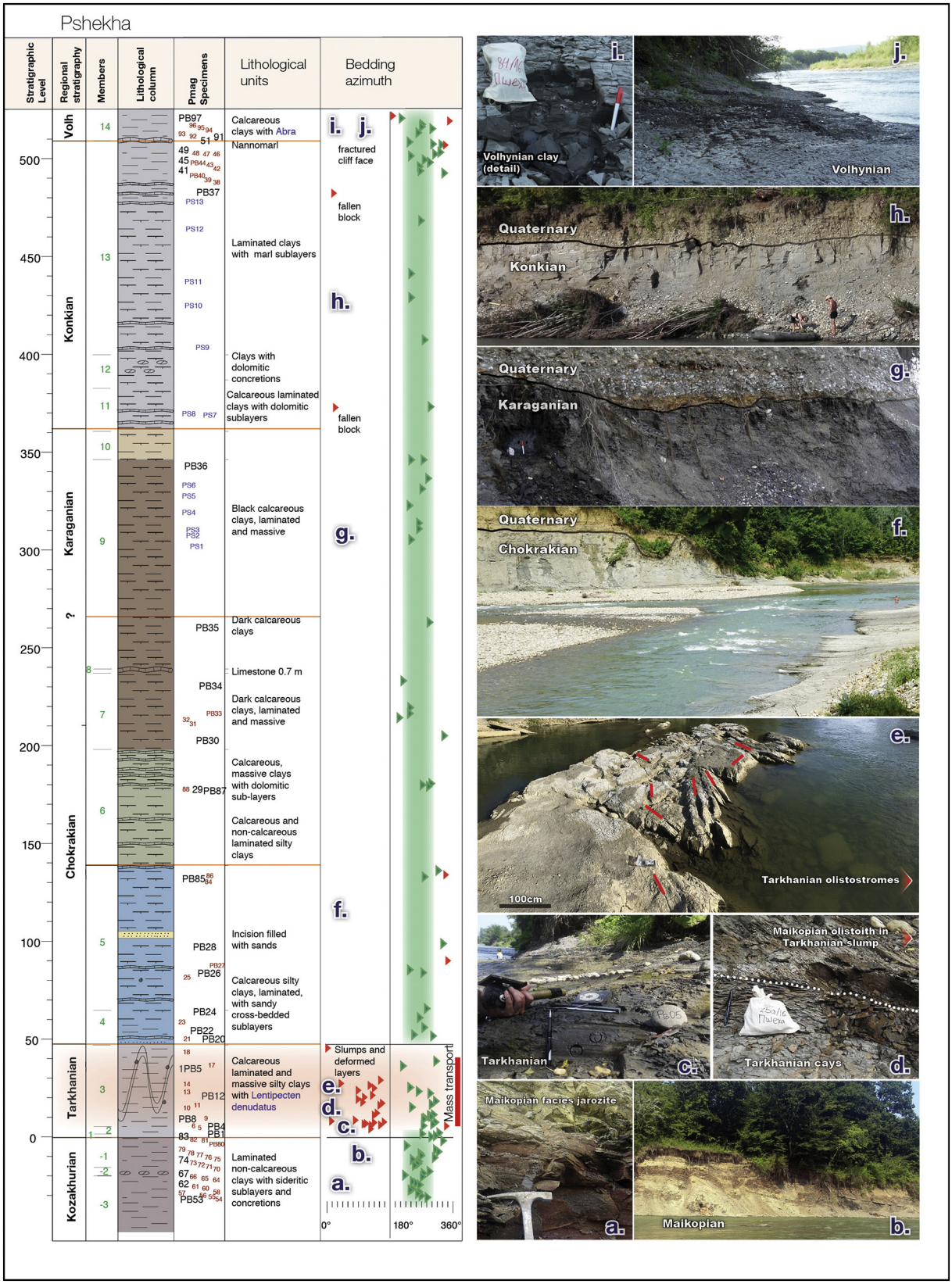

Fig. 6. Bio-lithostratigraphic overview of the Pshekha river section. Slump anomalies corresponding to the upper Tarkhanian stage revealed in the bedding anomalies.

the late Miocene (Beluzhenko et al., 2007; Akhmetiev et al., 1995; Sachsenhofer et al., 2017). The sediments are slightly tilted to the north and are accessible in the valley cuts of the rivers (Belaya, Pshekha, and many others). Here, we focus on the sections that display the transition from a monotonous sequence of anoxic clays of the Kozakhurian stage of the Maikop Series to the post-anoxic calcareous clays of the Tarkhanian and the algal bioherms of the Chokrakian.

The sections were logged in detail and sampled for biostratigraphic, paleomagnetic and geochemical purposes. Biostratigraphically we focus on mollusks, and calcareous nannoplankton assemblages that can be used to identify and locate the stage boundaries and to provide supplementary information on the environmental changes in the basin. Macrofossils are fully absent in the upper Maikopian part of the sections, but they are common and well preserved from the beginning of the Tarkhanian onwards, especially in the relatively shallow Belaya section. Nannoplankton was studied in the Tarkhanian part of the Pshekha section. We refer to the results of previous studies for the section along the Belaya river (Krasheninnikov et al., 2003; Golovina et al., 2009; Golovina, 2012). To identify nannofossils, smear slides were prepared using standard procedures (e.g. Golovina et al., 2004), which were examined under a Jena|Zeiss light microscope (cross and parallel nicols) at ×1200 magnification.

3.1. The Belaya section

The Kozakhurian-Volhynian succession is exposed along the Belaya river and its small tributaries (Fig. 4), roughly between Podgornyy (44°26′39.36″N/40°12′42.92″E) and Semikollenaya Ravine (44°32′58.95″N/40°08′24.91″E). The base of the studied section (Fig. 5) belongs to the top of the anoxic Maikop facies sediments (only 7.5 m is exposed). The uppermost Maikopian (Ritsa Fm) consists here of finely laminated, dark-brown, non-calcareous clays, devoid of macrofossils (Fig. 5.a). The transition to the Tarkhanian is gradual: first, carbonate/marl fragments appear in the sediments and then, in the uppermost two meters, the color slowly fades towards greyer tones, similar to the basal Tarkhanian clays.

The Tarkhanian sediments are very thin (~3 m) and consist of light grey, calcareous and non-calcareous clays with a very characteristic, 0.15 m thick, limestone layer known in literature as the "Tarkhanian marlstone" (Goncharova, 1989) in the middle part (Fig. 5b). The Tarkhanian contains a rich marine fauna assemblage with *Lentipecten denudatus* (Reuss), *Nucula nucleus* L., *Nuculana fragilis* (Chemn.), and *Aporrhais pespelicani* (L.). The Tarkhanian nannofossil record from Belaya is characterized by the appearance of abundant *Braarudosphaera bigelowii*, *Coccolithus pelagicus*, *Cyclicargolusus floridanus*, *Helicosphaera carteri*, *H. waltrans*, *H. mediterranea*, *Rhabdosphaera* sp., *Reticulofenestra pseudoumbilica* and *Sphenolithus heteromorphus* (Krasheninnikov et al., 2003; Golovina, 2012). Based on the joint presence of *Sphenolithus heteromorphus* and *Helicosphaera waltrans*, the assemblage can be correlated with Zone NN5 (Krasheninnikov et al., 2003; Golovina, 2012). The boundary with the overlying Chokrakian is sharp and somewhat irregular, which may be related to a gap in sedimentation, a disruption of sedimentation, or to the weight of the overlying Chokrakian bioherms.

The Chokrakian sediments (0–190 m) are significantly thicker and consist of stromatolitic bioherms alternating with clays and sands (Fig. 5.c). The lower part (0–60 m) comprises bryozoan dominated bioherms and light-colored clays; the upper part contains serpulid-dominated bioherms alternating with darker clays. Sands are only present in the middle and upper part of the succession (Fig. 5.d, e). The Chokrakian mollusks differ from the Tarkhanian assemblage by the presence of more euryhaline and endemic faunas. In the clay facies they reveal a poor association with *Varicorbula gibba* (Olivi), *Nuculana fragilis*, *Mactra bajarunasi* Kolesn., *Abra parabilis* (Zhizh.) and *Limacina andrusovi tschokrakensis* (Zhizh.). The bioherm facies is richer in mollusks and contains species like *Mytilaster volhynicus* (Eichw.), *Musculus conditus* (M. Hoern.), *Gregariella tarchanensis* (Gatuev), *Irus irus* (L.), *Ervilia praepodolica* (Andr.), *Gomphomarcia taurica* (Bajar.), *Chama toulai* David., *Nuculana fragilis* (Chemn.), *Arcopsis lactea* (L.), *Limaria (Limaria)* sp., *Parvicardium liverovskajae* (Merkl.). The sandy facies contain the most divers associations with *Anadara bosphorana* (David.), *Perna tschokrakensis* (Zhizh.), *Gomphomarcia taurica* (Bajar.), *Parvivenus marginata jusmaci* (Schwetz), *Macoma sokolovi* (Bajar.), *Pitar laskarevi* (Schwetz), *Europicardium pseudomulticostatum* (Zhizh.), *Parvicardium kubanicum* (Zhizh.), *Cerastoderma bogachevi* (Koles.), *Donax tarchanensis* (Bajar.), *Lutetia (Davidaschvilia) intermedia* (Bajar.), *Ervilia praepodolica* (Andr.) (according to Goncharova) and abundant gastropods. Most of the lower Chokrakian mollusks are not found in the upper Chokrakian (120–180 m), except for a couple of persisting endemics such as small *Lutetia intermedia* and *Ervilia praepodolica*. The topmost Chokrakian shows a shift to continental facies with plant and tree remains, coal beds and fragments of the terrestrial gastropods *Helix*, indicating a relative sea level fall/regression took place at the Chokrakian\Karaganian boundary.

The lithology of the relatively thick Karaganian deposits (190–375 m) is composed of clays and silts (Fig. 5f). The clays of the middle part (250–300 m) are containing levels with stromatolitic limestones (20–150 cm thick) while the upper part is sandier with limestone concretions. Fossils of *Davidaschvilia (Zhgentiana) gentilis* (Eichw.) dominate the lower Karaganian (190–310 m) mollusk associations, while *Savanella andrusovi* (Toula) rare *Barnea* and the gastropods *Mohrensternia*, are characteristic for the upper Karaganian (310–375 m). The Karaganian succession is conformably overlain by Konkian deposits.

The Konkian succession (375–525 m) consists of monotonous, poorly cemented, grey silts and grey-yellowish sands, occasionally interrupted by clay levels and sandstones (Fig. 5.g). The uppermost part of the Konkian comprises well-cemented carbonatic sandstones that are poorly exposed along the Belaya River but are properly outcropping in the valleys of the east side tributaries. From the faunal point of view, the lowermost Konkian is distinguished by the appearance of the genus *Ervilia* and *Barnea* sharp domination. Higher up in the succession also *Ervilia trigonula*, *Davidaschvilia (Zh.) gentilis* (Eichw.), *Savanella andrusovi*, *Barnea pseudoujratamica* (Ossip.), and *Cerastoderma praeplicatum* (Hilb.) are present. The Konkian (Sartaganian and Veselyankian parts) contains more divers marine mollusk faunas: genus *Limacina* and *Chlamys* sp., *Mactra basteroti konkensis* (Sok.), *Parvivenus konkensis* (Sok.), *Nassarius reticulatus*, *Acanthocardia andrusovi* (Sok.), *Varicorbula gibba*, and *Anomia ephippium*. Previous studies concerning the Konkian/Volhynian foraminifera and calcareous nannofossils from the Fars and Belaya rivers have been performed by Vernyhorova Yu. and Golovina L. (Golovina et al., 2009). The rich foraminifera assemblages contain a large number of normal-marine foraminifera species typical of Konkian sediments: *Discorbis kartvelicus*, *Angulogerina angulosa*, *Globulina gibba*, *Virgulina schreibersiana*. The nannoplankton assemblages are represented by *Coccolithus pelagicus*, *Cyclicargolithus floridanus*, *Braarudosphaera bigelowi*, *Rhabdosphaera sicca*, *Rhabdosphaera poculi*, *Reticulofenestra pseudoumbilicus*, *Helicosphaera carteri*, *Holodiscolithus macroporus*, *Pontosphaera multipora*, *Thoracosphaera* sp. According to the taxonomic composition, the nannoplankton assemblages of the Fars and Belaya sections, are almost identical to the assemblages of the Sartaganian beds in the Zelensky section (Taman Peninsula; Palcu et al., 2017).

The Volhynian deposits conformably overlie the Konkian sediments. The very base of the Volhynian is marked by silts and sands, but these are sharply followed by a thick monotonous series of grey clays that extends throughout the rest of the Volhynian succession (Fig. 5.h). Faunistically, abundant *Abra* in and *Mactra* fossils are present in the Volhynian.

3.2. The Pshekha section

A deeper water analogue of the Maikopian-Volhynian succession of Belaya is exposed in the valley cut of the Pshekha river (Fig. 4), between Shirvanskaya Vodokachka (44°21′50.87″N/39°47′38.10″E)

and Tsurevskiy (44°24′49.27″N/39°47′27.08″E). The exposed Maikopian part of the Pshekha section is 40 m thick and comprises a more diverse succession of finely laminated, dark-brown, non-calcareous clays, with manganese-dolomitic concretions and secondary sulphate-rich levels (Fig. 6.a, b). Like in Belaya these deposits are devoid of macrofossils.

The Tarkhanian deposits (0–47 m) that follow conformably in the sedimentary succession consist of light-grey to dark-grey carbonatic clays (Fig. 6.c). A large part of the succession (~35 m), however, is represented by a massive olistostrome (Fig. 6.d, e) and slumps. The olistoliths are composed of large fragments of Maikopian clay and deformed Tarkhanian clays. The uppermost levels of the Tarkhanian show limited to no deformation, indicating that the transition to the Chokrakian is conformable, and that the main slumping event took place in the middle-upper Tarkhanian. Macrofaunistically, the Tarkhanian is characterized by the presence of *Lentipecten denudatus*. New nannoplankton studies have been performed on 12 samples from the Tarkhanian and lower Chokrakian part of the section.

The first nannofossils appear in the lower Tarkhanian and consist of *Reticulofenestra* sp., *Reticulofenestra pseudoumbilicus* and *Reticulofenestra* cf. *minuta*. Overall, the nannofossil assemblage of the Tarkhanian is characterized by the absence of *Helicosphaera ampliaperta* and the presence of *Sphenolithus heteromorphus* and *Helicosphaera waltrans* - which gives grounds to correlate the nannofossil assemblage with the NN5 Zone. In addition, *Helicosphaera carteri* is relatively abundant, *H. euphratis* (very rare), *Rabdosphaera pannonica*, *Cyclicargolithus floridanus* and the genera *Umbilicosphaera* and *Calcidiscus* are present, and the genera *Discoaster* is absent.

The Chokrakian (47–270 m) is estimated to be ~220 m thick and consists of clays with sandy and dolomitic sub-layers, rhythmically interrupted by marly intercalations, and stromatolitic calcareous crusts. A notable feature in the lower part of succession is the presence of an incised channel, filled with sands (Fig. 6.f). Similar to Belaya, there is strong change in color from light grey-greenish clays in the lower Chokrakian to dark grey clays in the upper Chokrakian.

The lower Chokrakian is characterized by few in situ nannofossils and abundant redeposited species of Paleogene age. *Helicosphaera waltrans* and *Sphenolithus heteromorphus* are absent here. Higher in the section, the assemblage is characterized by the common presence of *Sphenolithus heteromorphus*, but *Helicosphaera waltrans* is absent.

The Chokrakian/Karaganian boundary is hard to determine in the Pshekha section due to the lack of faunal markers. We place it at ~270 m, after the dolomitic/limestone layers that are tentatively correlated with the Chokrakian bioherms and limestones in Belaya. The Karaganian (~270–360 m) is dominated by dark calcareous clays without macrofossils (Fig. 6.g), except for a single finding of *Davidaschvilia (Zh.) gentilis*.

Further up in the section, the Konkian (~150 m thick) and Volhynian (of which only ~10 m have been investigated) are characterized by grey clayey facies with limited lithological and faunal markers (Fig. 6.h–j). The base of the Konkian is placed at a change in lithology – from dark clays to rhythmic alternations of grey clays and dolomitic sub-layers. The top of the Konkian shows the sedimentation of the coccolithic laminated nannoplankton-rich marl represented by monospecific *Reticulofenestra pseudoumbilicus* almost identical to one from the top of Konkian in the Zelensky section (Taman Peninsula – Golovina et al., 2004; Palcu et al., 2017). The Volhynian is recognizable by the presence abundant *Abra reflexa* level.

4. Magnetostratigraphy and radio-isotope dating

Magnetostratigraphy can provide ages to rock successions if the established polarity pattern of the studied sections can be correlated to reversal pattern of the Geomagnetic Polarity Time Scale (e.g., Langereis et al., 2010). Previous applications of this approach have been proven successful on Paratethyan sediments, if adequate demagnetization techniques are applied to deal with the generally high concentration of iron sulphides in anoxic sediments, and in particular with the magnetic mineral greigite (Vasiliev et al., 2008, 2010; Paulissen et al., 2011; De Leeuw et al., 2013; ter Borgh et al., 2013; Palcu et al., 2015, 2017; Van Baak et al., 2016; Liu et al., 2017; Kelder et al., 2018). The Belaya and Pshekha sections were sampled at a resolution that varies from centimeters to meters-scale with a hand-held electric drill using water as a coolant. Paleomagnetic cores were collected from a total of 264 levels (154 from Belaya and 110 from Pshekha). The orientation of the paleomagnetic cores and the corresponding bedding planes were obtained using a magnetic compass, previously corrected for the local magnetic declination.

4.1. Rock magnetism

In the laboratory of Fort Hoofddijk, rock-magnetic tests were conducted to understand the nature of the magnetic carriers. These tests include measurements of hysteresis loops, first-order-reversal-curve (FORC) diagrams, and thermomagnetic runs in air. Hysteresis loops (sample mass 60–90 mg) were measured with a Princeton Measurements Corporation MicroMag 2900 alternating gradient magnetometer (AGM, noise level 2×10^{-9} A m^2) between −1 T and 1 T with field increments of 10 mT. The saturation magnetization (Ms), the saturation remanent magnetization (Mrs), coercivity (Bc) were acquired after correction for the paramagnetic slope (at 70% of the maximum field). Back field demagnetization of SIRM was performed after saturating the sample in a field of 1 T to determine the remanence coercivity (Bcr). For first-order reversal curves (FORCs), 150 reversal curves were obtained for each sample with a field increment of 1.5 mT. FORC diagrams were calculated using the FORCinel Program Version 1.19 (Harrison and Feinberg, 2008). All the measurements on the AGM were performed with an averaging time of 200 ms. High-temperature thermomagnetic measurements of the induced magnetization (J-T curves) were performed in air with a modified horizontal translation-type Curie balance with a sensitivity of ~$5 * 10^{-9}$ A m^2 (Mullender et al., 1993). About 70 mg of powdered sediments were positioned in a quartz glass holder. The applied field was cycled between 100 mT and 300 mT. Multiple heating and cooling runs were performed between room temperature, 150, 250, 350, 450, 525, 700 °C. The heating rate was 6°/min and the cooling rate was 10°/min.

In terms of rock magnetic properties, the samples were divided into two types: type 1 samples have high magnetic coercivities (>30 mT, Fig. 7.a) and high ratios of Mrs/Ms and Bcr/Bc. Their FORC diagrams (Fig. 7c) have classic SD-like contours centered on Bc ~50 mT, which is similar to those previously reported for SD diagenetic greigite (Roberts et al., 2011, 2006). The central peak is not symmetrical with respect to the Bu axis but shifted to negative values. For the J-T curves (Fig. 7.e), all the magnetically strong samples show an irreversible decrease in magnetization between 200 °C and 350 °C, which is typical of greigite (e.g. Dekkers et al., 2000). Pyrite also exists in these samples, indicated by the magnetization increase after 400 °C (due to its oxidation via magnetite ultimately to hematite) (Passier et al., 2001).

Type 2 samples are dominated by paramagnetic minerals, as suggested by the essentially linear magnetization curve before paramagnetic correction. After correction, the samples show a low coercivity ~10 mT (Fig. 7.b). Due to the low intensity (two orders of magnitude lower than the type 1 samples), only a weak FORC distribution is observable (Fig. 7.d). The J-T curves of these magnetically weak samples are reversible during thermal runs below 400 °C. The increases after 400 °C indicate large amounts of pyrite in these samples, which oxidize to magnetite causing the peak at 450–500 °C in J-T curves (Fig. 7.f). Abundant pyrite in these samples is also consistent with the low intensity and subtle hysteresis since pyrite is paramagnetic. The distributions of the type 1 and type 2 carriers throughout the section do not match a lithological pattern or the polarity changes which suggests primary directions are preserved by both carriers.

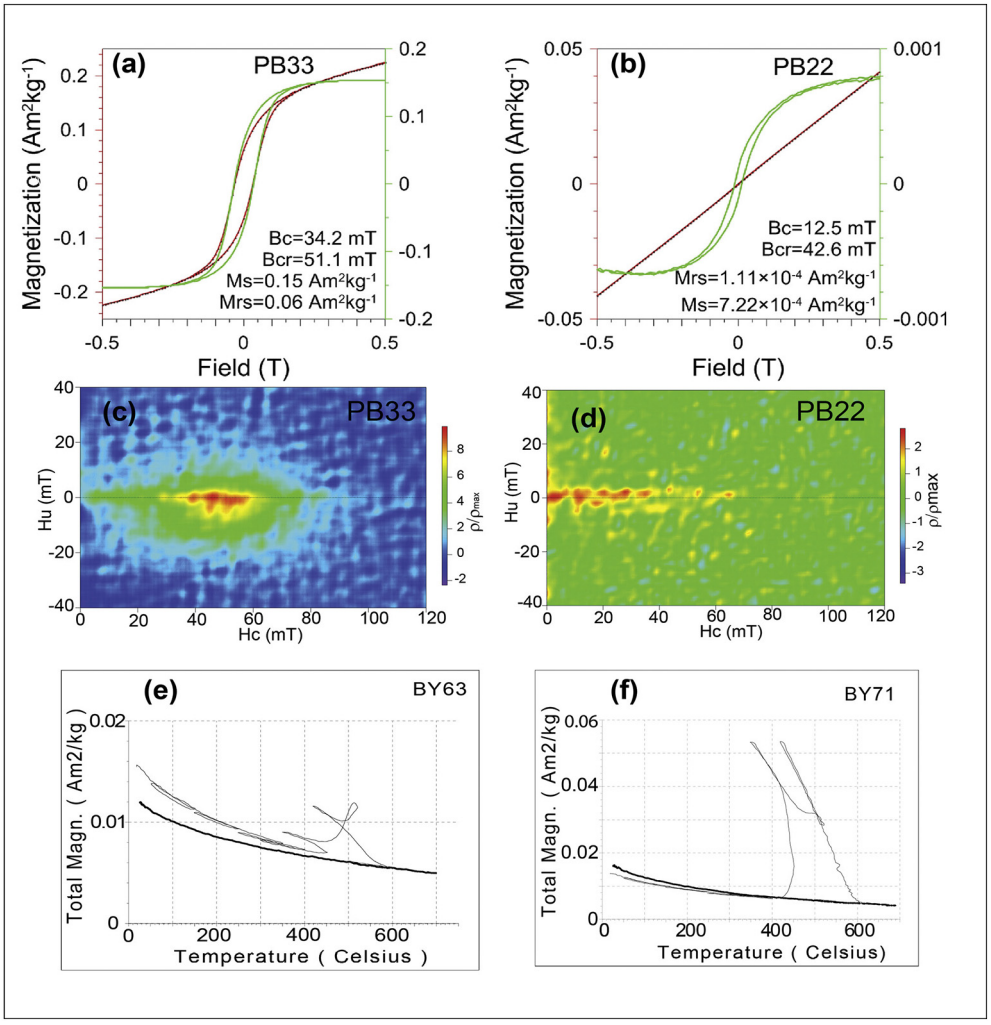

Fig. 7. Rock magnetic properties of type 1 (a, c, e) and type 2 (b, d, f) samples. Hysteresis loops (measured up to ±1 T) are zoomed in to show the central portion in (a) and (b). The red lines and green lines indicate results before and after paramagnetic correction, respectively. Hysteresis parameters obtained from the hysteresis loops (after paramagnetic correction), IRM acquisition and direct-current field demagnetization curves are shown alongside. (c) and (d) are FORC diagrams generated with a smoothing factor of 5. (e) and (f) are J-T curves measured on the Curie Balance. The thin line represents multiple heating and cooling runs before reaching the highest temperature (700 °C), while the thick line represents the last cooling from 700 °C to room temperature.

4.2. Demagnetization and magnetic polarity patterns

Subsequently, thermal and alternating field demagnetization techniques were applied to isolate the characteristic remanent magnetization (ChRM). The Natural Remanent Magnetization (NRM) was thermally demagnetized and measured using a 2G Enterprises DC Squid cryogenic magnetometer (noise level of $3 * 10^{-12}$ A m^2). The heating was performed in a magnetically shielded furnace, with a residual field less than 10 nT. The thermal steps were based on the behavior of samples during thermomagnetic runs, with relatively small temperature increments of 10–30 °C applied in the 100–360 °C range because of the rapid thermal decay and the occurrence of additional secondary magnetic carriers after 400 °C. In addition, alternating field demagnetization was performed, with small field increments, up to a maximum of 100 mT with an automated sample handler, attached to a horizontal 2G Enterprises DC SQUID cryogenic magnetometer (Mullender et al., 2016).

The NRM intensity ranges between $16 * 10^{-6}$ A/m and $20 * 10^{-1}$ A/m for the Belaya section and between $28 * 10^{-6}$ A/m and $29 * 10^{-1}$ A/m for the Pshekha section (Fig. 8). We identified the ChRM by analyzing the decay-curves and vector end-point diagrams (Zijderveld, 1967). During both the progressive thermal demagnetization and the progressive alternating fields demagnetization, two magnetic components can be recognized. A very weak, low-temperature, viscous overprint is generally removed at 120 °C and 15 mT (Fig. 8). A second, higher-temperature, component has been removed at temperatures between 120 °C and 300 °C, and alternating fields of 15–50 mT. This component is of dual polarity and is interpreted as the ChRM. The ChRM directions were defined by at least four consecutive temperature steps and calculated with the use of principal component analysis (Kirschvink, 1980).

We use the maximum angular deviation (MAD) of the calculated directions to separate the results into three quality groups. The 1st quality (MAD = 0–5) and 2nd quality groups (MAD = 5–10) have been used for determining the polarity patterns (Fig. 8). The 3rd quality results (with contradictory declinations and inclinations related to confirmed disturbed/slumped sediments and olistoliths) do not represent primary directions (Fig. 8). The ChRM directions and magnetic intensity have all been plotted against stratigraphic levels (Fig. 8). The polarity pattern of the Belaya section comprises fourteen different polarity intervals, seven of reverse (bR1-7) and seven of normal (N1-7) polarity. The polarity pattern of the Pshekha section comprises fourteen different polarity intervals, seven of reverse (pR1-7) and seven of normal (pN1-7) polarity.

Some anomalies have been encountered in each section. Paleomagnetic anomalies, (bN2a, Fig. 8.b) are especially present in the base of the

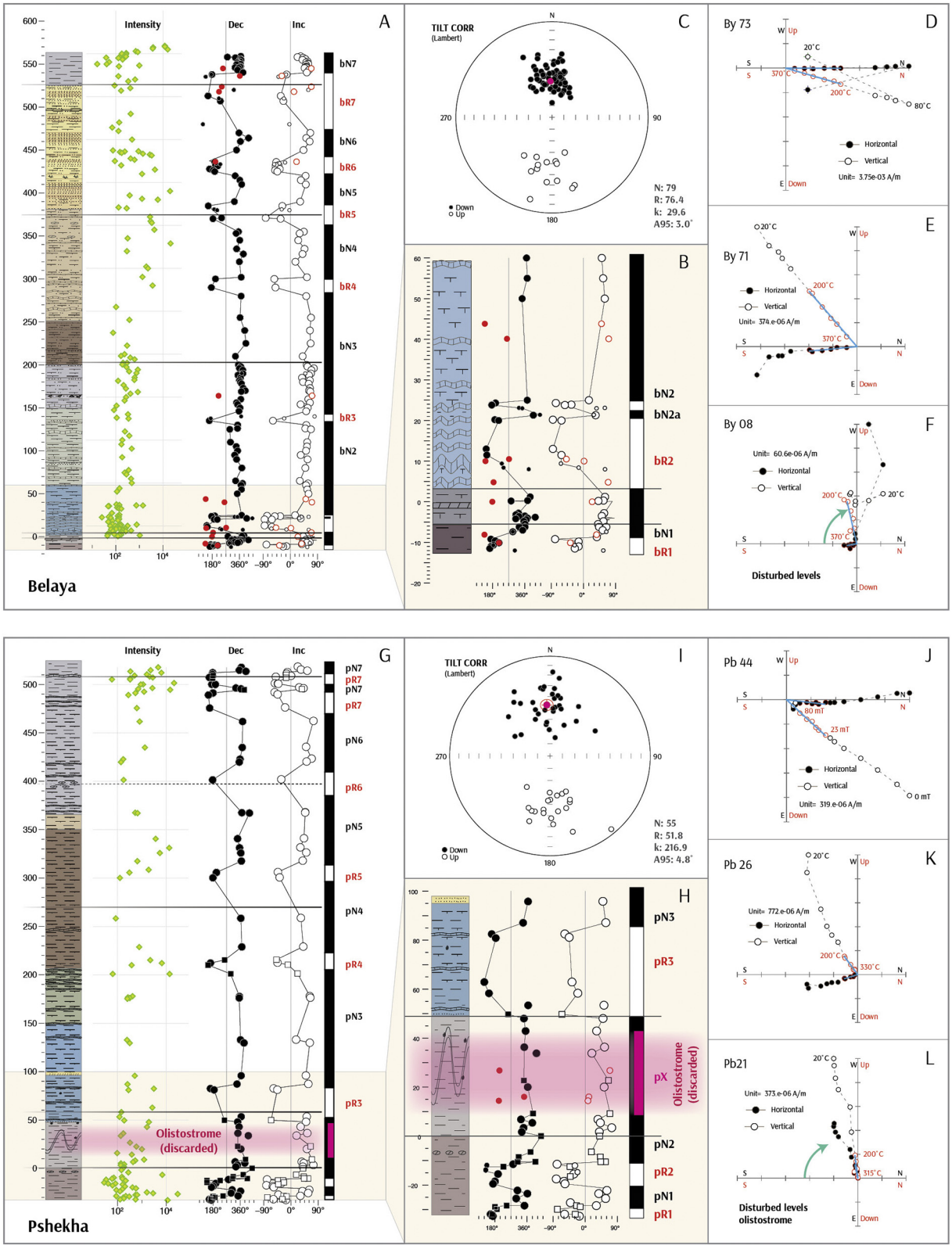

Fig. 8. Schematic lithological column, magnetic intensity and polarity zones, stereo plots and Zijderveld diagrams for the Belaya and Pshekha sections. Seven reversed polarity intervals (R1–R7) and seven normal ones (N1–N7) have been identified in both in the Belaya (A, B) and Pshekha (G, H) section. The positions of the stage boundaries are marked with black lines. Representative examples of Zijderveld demagnetization diagrams after tilt correction (Belaya - D, E, F; Pshekha - J, K, L), please note the disturbed levels corresponding to slumps and mass transport (F, L). Sample codes are specified in the upper corner. Filled (unfilled) circles represent the projection on the horizontal (vertical) plane. The red-outlined temperature values represent interval used for calculating the ChRM component which is marked by the blue line. The stereographic plots (C, I) show the antipodal distribution of the ChRM directions.

Belaya and Pshekha sections, related to slumps, olistoliths and other forms of mass transport (pX, Fig. 8.h).

4.3. Radio-isotope dating

In the Belaya section a volcanic ash level occurs at 120 m (BY55) in the Chokrakian stage (Fig. 5). We separated biotite (125–250 μm) from this level by washing and sieving, followed by standard heavy liquid ($\rho > 3.0$ g/cm^3) and magnetic separation procedures. A final fraction of this sample was hand-picked under an optical microscope. The sample was wrapped in Al-foil and irradiated together with Fish Canyon sanidine standard for 7 h in the Oregon State University CLICIT facility, USA. After irradiation samples and standards were loaded in a 185-hole tray and placed in a vacuum chamber connected to a preparation line equipped with 3 NP10 getters and an Argus VI+ noble gas mass spectrometer. Multiple crystal aliquots (~3–10 grains) were fused using a CO_2 laser and analyzed with the following collector settings: H2 Faraday cup with 10E12 Ohm amplifier for m/e 40, H1, L1, and L2 Faraday cups with 10E13 ohm amplifiers for m/e 39, 38 and 37 and a compact discrete dynode (L2) for m/e 36. Similar to Phillips and Matchan (2013) we did not apply bias corrections, but analyzed samples and standards alternating with air pipettes of different intensities in the same range as the samples and standards. Line blanks were measured every 2–3 unknowns and were subtracted from succeeding sample data. Data reduction is done in ArArCalc (Koppers, 2002). Ages are calculated with Min et al. (2000) decay constants and 28.201 ± 0.022 Ma for FCs (Kuiper et al., 2008). The atmospheric air value of 298.56 from Lee et al. (2006) is used. The correction factors for neutron interference reactions are $(2.64 \pm 0.02) \times 10^{-4}$ for $(^{36}Ar/^{37}Ar)_{Ca}$, $(6.73 \pm 0.04) \times 10^{-4}$ for $(^{39}Ar/^{37}Ar)_{Ca}$, $(1.21 \pm 0.003) \times 10^{-2}$ for $(^{38}Ar/^{39}Ar)_{K}$ and $(8.6 \pm 0.7) \times 10^{-4}$ for $(^{40}Ar/^{39}Ar)_{K}$. All errors are quoted at the 1σ level and include all analytical errors.

In the field we found evidence for potential reworking of the biotite and therefore we tried to analyze the lowest amounts of grains possible in a single fusion step. We performed 10 analyses of 3 grains per fusion. We added another 25 analyses with ~10 grains per fusion. Fig. 9 shows the heterogeneous age distribution with a spread in ages between 4 and 36 Ma with median peak around ~14.8 Ma. The radiogenic amount of ^{40}Ar ranges from almost 0 to 82% and only 10 analyses yield >50% $^{40}Ar^*$ (Fig. 9). Low radiogenic argon contents might suggest alteration and open system behavior and argon loss. This will result in younger ages than its original eruption age. On the other hand, potential reworking during transport and/or xenocrystic contamination can yield heterogeneous age populations with a bias to ages older than eruption age. The age of this ash is ~14.3–14.4 Ma according to our magnetostratigraphic age model, and although the $^{40}Ar/^{30}Ar$ data are complex as discussed above, they do not contradict our age model.

5. Magnetostratigraphic age model for the Tarkhanian-Chokrakian stages of Eastern Paratethys

We aim to obtain a time frame for the Kozakhurian-Tarkhanian-Chokrakian-Karaganian deposits of Eastern Paratethys by correlating the observed polarity pattern of the Belaya and Pshekha sections to the astronomically dated polarity time scale of the most recent GPTS (Hilgen et al., 2012) (Fig. 10). The polarity patterns of the Belaya and Pshekha sections are in good agreement.

The Kozakhurian-Tarkhanian part in the Pshekha section (excluding the slumped interval) is marked by two small reversed intervals (pR1 and pR2) alternating with two small normal intervals (pN1 and pN2), with the entire Tarkhanian in pN2. In Belaya, the Tarkhanian also corresponds to a small normal interval (bN1) that is followed by one small reversed interval (bR2), indicating that bN1 corresponds to pN2. In both sections the Chokrakian is marked by a small reversed interval at the base (bR2/pR3) followed by two much larger normal intervals (bN2-3 and pN3-4) that are separated by a very short reversed interval

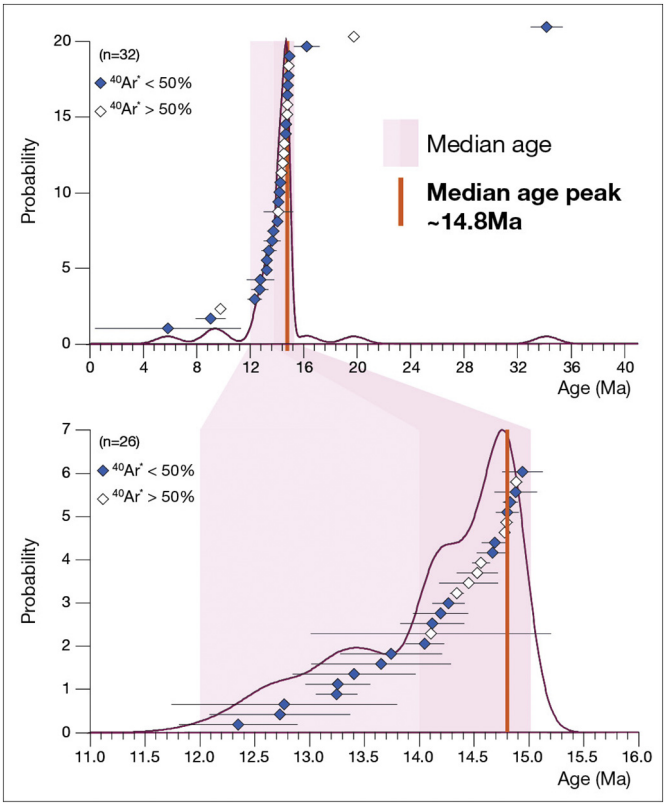

Fig. 9. Radio-isotope dating results.

(bR3/pR4). The Chokrakian-Karaganian boundary is in both sections located in the second large normal interval (bN3/pN4), with the notification that in Pshekha this boundary is not very well constrained. The Karaganian-Konkian interval comprises in both sections three additional normal intervals (bN4-6 and pN5-7) after which the base of the Volhynian is located in a reversed interval (bR7/pR8).

Regarding previous age estimates and correlations to geological time scales, the studied succession most probably corresponds to the age interval between 17 and 12 Ma (e.g. Nevesskaya et al., 2005a; Piller et al., 2007; Hilgen et al., 2012). A conspicuous feature of this interval is the presence of the very long reversed chron C5Br between 16 and 15.2 Ma (Fig. 10), which is missing in the magnetostratigraphic pattern of our two sections. The logical solution explaining the absence of C5Br is a correlation to the younger part of the time scale, e.g. between 15 and 12.5 Ma.

The polarity patterns of Belaya and Pshekha are both marked by the presence of four relatively large normal polarity intervals separated by smaller reversed polarity intervals (bN2-bN5/bR3-bR6 and pN3-pN6/pR4-pR6) that correlate very well with chrons C5ADn-C5AAn. The two normal polarity zones of the Karaganian stage (bN3-4/pN4-5) then correlate with C5ACn and C5ABn respectively, in agreement with the previous magnetostratigraphic results of Taman (Palcu et al., 2017). Correlating downwards, bN2/pN3 corresponds to C5ADn; bN1/pN2 to C5Bn.1n and finally pN1 correlates with C5Bn.2n. The Kozakhurian/Tarkhanian boundary (bN1/pN2) is located in the middle part of chron C5Bn.1n (14.775–14.87 Ma) and has a corresponding age of ~14.85 Ma.

The Tarkhanian/Chokrakian boundary, located just above the polarity reversal bN1/bR2 and pN2/pR3, is determined just above the C5Bn.1n/C5ADr polarity reversal (14.775 Ma) and has an age of ~14.75 Ma. The Chokrakian/Karaganian boundary is best constrained in Belaya and corresponds to chron C5ACn and an age of 13.9–13.8 Ma. The changing lithology (clear coarsening up trend and the presence of bioherms) complicates a more precise age estimation. The Karaganian/Konkian

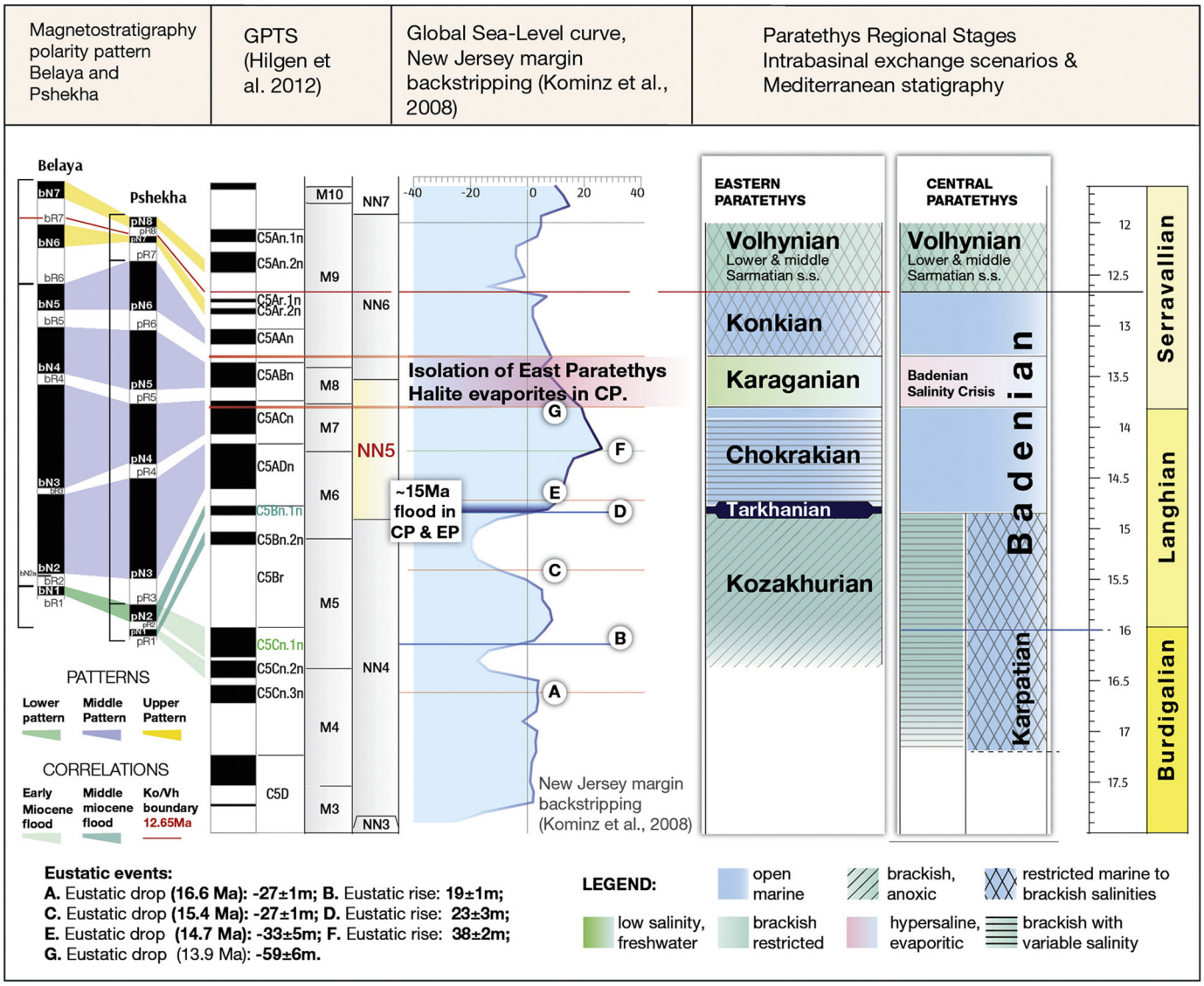

Fig. 10. The age model of the Belaya and Pshekha sections and the global sea-level fluctuations. Stratigraphic correlations between the Central Paratethys, Eastern Paratethys and Mediterranean stages.

boundary in Belaya correlates to C5AAr and an age of 13.3 Ma, which is ~1 kyr younger than in Taman (13.4 Ma; Palcu et al., 2017). The Konkian/Volhynian boundary is located in a reversed interval that we correlate to C5An.2r, assuming it is synchronous with the Taman succession and the Badenian-Sarmatian extinction event (Palcu et al., 2015, 2017). This latter correlation implies that the very short polarity intervals C5Ar.1n and C5Ar.2n are not fully recovered in our magnetostratigraphic sampling.

We do not see a logical alternative correlation between the Tarkhanian-Karaganian magnetostratigraphic patterns of Belaya and Pshekha and the GPTS unless one assumes dramatic changes in the sedimentation rate and/or significant hiatuses. Regarding the alternative age estimate of ~16 Ma for the base of the Tarkhanian (Hilgen et al., 2012), this would only be possible if there is a ~1 Myr hiatus in both sections, for which we do not see any evidence.

Following our new age model, we can calculate the average sediment accumulation rates for both sections. These are 26 cm/kyr for Belaya and 28 cm/kyr for Pshekha. Maximum values are 44 cm/kyr in Belaya and 49 cm/kyr in Pshekha, both corresponding to the Karaganian. Minimum values (9–19 cm/kyr) correspond to the Kozakhurian in Pshekha and the top Kozakhurian-Tarkhanian in Belaya, respectively.

6. Discussion

6.1. The shutdown of an anoxic giant

We have provided new evidence that the termination of anoxic conditions in the Maikop Sea took place at 14.85 Ma, corresponding to the Tarkhanian flooding of the Eastern Paratethys. This is in good agreement

Fig. 11. The race between tectonic uplift, sea-level change and erosion shapes paleoenvironments. The Paratethys example: a. The initial state during the ***Kozakhurian***; b. The ***Tarkhanian*** regional stage (14.85–14.75 Ma) corresponds to the peak of the middle Langhian sea-level rise that flooded Central Paratethys that overcomes uplift; c. The ***Karaganian*** stage (13.9–13.4 Ma) represents a phase of loss of connectivity in the context of sea-level drop and uplift in the gateway area, d. Extrapolation of the size of the Carasu Strait, based on the global eustatic level curve (Kominz et al., 2008) and the degree of restriction observed in the EP environments.

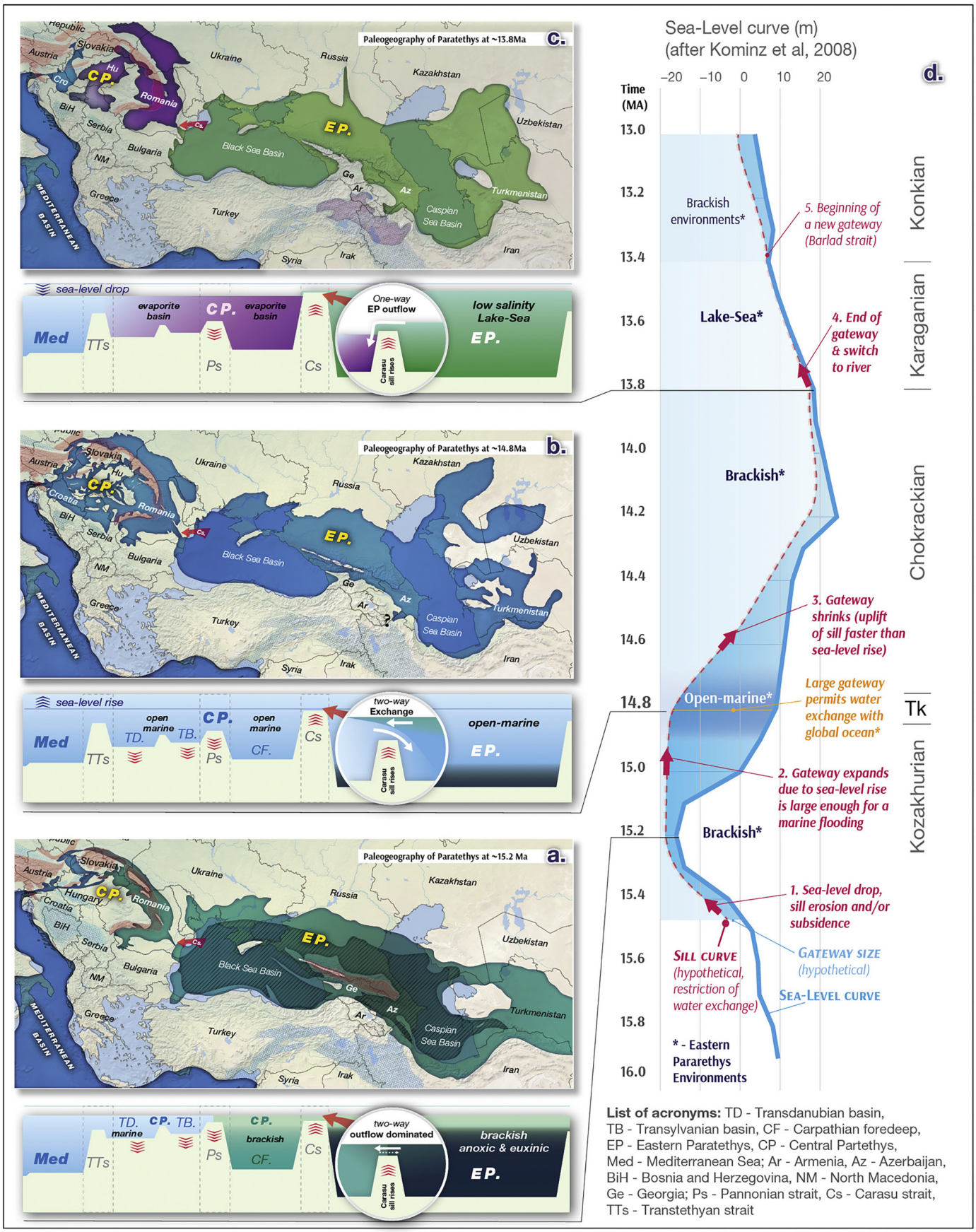

List of acronyms: TD - Transdanubian basin, TB - Transylvanian basin, CF - Carpathian foredeep, EP - Eastern Paratethys, CP - Central Partethys, Med - Mediterranean Sea; Ar - Armenia, Az - Azerbaijan, BiH - Bosnia and Herzegovina, NM - North Macedonia, Ge - Georgia; Ps - Pannonian strait, Cs - Carasu strait, TTs - Transtethyan strait

with previous correlations that place the Tarkhanian flood within the NN5 zone (Konenkova and Bogdanovich, 1994) or at the base of the NN5 zone (Ivanova, 1999, Barg and Ivanova, 2001). Key element from the nannoplankton point of view is the presence of *H. waltrans* in Tarkhanian successions, which has its FO at 15.5 Ma in the Mediterranean Sea. According to Sant et al. (2017), Kováč et al. (2007) and Kovac et al. (2018), *H. waltrans* first appears in the Central Paratethys together with *P. glomerosa* at an age <15.2 Ma, during the Badenian flooding of the Carpathian foredeep. The large resemblance of Tarkhanian faunas with early Badenian faunas of the Central Paratethys (e.g. Popkhadze, 2016) suggests an eastward marine transgression that flooded Central Eurasia reaching as far as the Eastern Paratethys (Figs. 11.b, 12). This paleogeographic setting makes the Eastern Paratethys the most peripheral basin and the first to lose its marine character when connectivity becomes restricted.

Various earlier attempts to correlate the Tarkhanian flooding of the Eastern Paratethys with global events have assumed a much older age for the base of the Tarkhanian. Many authors agree that a middle Miocene transgression occurred at the base of the Langhian reconnecting the Mediterranean with the Central and Eastern Paratethys (Nevesskaya et al., 1984; Nevesskaya et al., 1986; Iljina, 1995; Jones and Simmons, 1996; Cicha et al., 1998). The Tarkhanian stage has also been also correlated with the upper part of the Lower Miocene because the underlying Maikopian (Kozakhurian) deposits have common endemic mollusks with the upper Ottnangian stage of Central Paratethys (Popov and Voronina, 1983). The range of the age estimates for this event (16.8–16.0 Ma) reflects the changes in the definition of the base Langhian age. It is in this respect important to notice that although many authors suggest a transgression at the base of the Langhian in most sub-basins of the Central Paratethys, except for Austria and southwestern Hungary, the marine Badenian flooding occurred in the middle Langhian, estimated at ~14.7 Ma (Kováč et al., 2007) or between 15.1 and 14.9 Ma (Sant et al., 2017, 2018) instead of ~16.0 Ma. Consequently, a marine flooding of the Eastern Paratethys at ~16 Ma requires the presence of an alternative marine gateway, e.g. to the Indian Ocean, which has indeed been proposed for Tarkhanian times (e.g. Rögl, 1998).

The new magnetostratigraphic data from the Belaya and Pshekha sections indicates that the hypothesis of a ~16 Ma old Tarkhanian transgression requires a very large gap of ~1.4 Myr in both successions. Traditionally, seismo-stratigraphic data in Eastern Paratethys observe a regional scale unconformity at the Kozakhurian/Tarkhanian transition (Bobylev and Pishvanova, 1979). This unconformity, known as the "upper Maikopian disconformity", can be observed on many seismic profiles both in deep-water facies and in shallow/peripheral zones of the Eastern Paratethys. However, continuous sedimentary transitions have also been reported from sections in Malyi Kamislak and Crimea (Andreyeva-Grigorovich and Savytskaya, 2000). Recently, Ruban et al. (2010) describe a short-lived unconformity in the Tarkhanian, but they note that it corresponds to a disturbance in sedimentation and not to an erosional boundary. In both Belaya and Pshekha sections we interpret the succession as relatively continuous, with no erosional features that could be interpreted as significant gaps in the record. Coarse sediments such as gravels or conglomerates are lacking. No elements of sub-aerial deposition, no erosional features such as canyons and no sharp angular unconformities are present. Both records have disturbed bedding, however, in the levels that correspond to the upper Tarkhanian. Slumps synchronous with sedimentation in the deeper depositional setting and relatively reduced thickness in the more marginal section suggest a short-lived disturbance in the sedimentation, due to an episode of instability in the basin for reasons that are yet to be explained.

The magnetostratigraphic records of Belaya and Pshekha provide a straightforward correlation of the Tarkhanian to chron C5Bn.1n. The base of the Tarkhanian is consequently dated at 14.85 Ma. We conclude from our new magnetostratigraphic data that the previously envisaged scenario with an "old" Tarkhanian flooding, beginning at ~16.2–16.0 Ma and fueled by the Indian Ocean, is very unlikely, although not completely impossible.

6.2. Paleogeography of the Tarkhanian-Chokrakian gateway(s)

Several gateway configurations have been proposed for the faunal exchanges that occurred in the Tarkhanian and to a certain extent in the Chokrakian. These gateway configurations are difficult to test, for the Tarkhanian stage alone, as it is very short. Therefore, we consider the gateway systems that functioned throughout the Tarkhanian and Chokrakian.

A marine connection to the Indian Ocean, via Iran, has been proposed by various authors (Rögl and Muller, 1976; Steininger et al., 1978) in the attempt to justify the presence of so-called Indo-Pacific faunal elements in the Tarkhanian. However, other studies question the direct relationship between the middle-late Miocene Paratethyan fauna and the Indo-Pacific fauna and consider the similarities as due to relict Tethyan characteristics preserved from Oligocene-Early Miocene (e.g. Kokay, 1985; Harzhauser et al., 2002). From the paleoenvironmental point of view, magnetostratigraphic and radio-isotope dating of the sediments of the Iranian Plateau, in NW Iran, (Ballato et al., 2017) show that already from 16 Ma onwards this basin had a continental character (playa lakes and braided rivers). Similarly, the Qom basin, in central Iran, retains continental characteristics (the upper red formation) from upper Burdigalian (>16 Ma) onwards (Reuter et al., 2009). A gateway via the Sivas Basin, in Eastern Turkey can also be discarded as recent studies show that middle Miocene deposits in the region only represent continental environments (Poisson et al., 2016). A northward extension of the Tethys Gateway in Easternmost Turkey is also excluded as the last marine deposits stretching from the Tethyan Gateway towards North (north of the Bitlis–Poturge Massif) are of Oligocene age (Hüsing et al., 2009).

The presence of Central Paratethyan elements in Eastern Paratethys, however, is unequivocal (Popkhadze, 2016) and two possible gateways have been proposed: the Dniepr and Carasu Straits. We consider a connection via the Dniepr Strait as highly unlikely as the faunas of the age-equivalent (Early Badenian, Chokrakian) deposits from the two sides of the proposed gateway show no similarities in faunal elements (Goncharova and Il'ina, 1997). The Carasu Strait, located in the SE of present-day Romania, shows a West-East gradient of Badenian to Chokrakian fauna (Chiriac et al., 1969) and is the most likely transit pathway between Central and Eastern Paratethys. The deposits are very limited in thickness (~2 m), which justify the fact that the Tarkhanian has not yet been properly described. We consider this gateway as the only viable candidate for the Tarkhanian flood and, though we cannot exclude the existence of other gateways, the Carasu Strait must certainly have played a pivotal role in the faunal transfer between from Central to Eastern Paratethys.

6.3. Mechanisms affecting gateway functioning at the end of anoxia

Tectonics and sea-level fluctuations have major influence on the functioning of gateways. The result of this tectono-eustatic interplay is best observed in the paleoenvironmental changes in marginal seas such as the Paratethys realm. Unraveling this complex interaction is challenging because only the eustatic sea level record has been accurately dated while time scales for tectonics in the gateway regions lack the adequate resolution for a straightforward correlation. Our new chronology for the connectivity episodes allows overcoming this issue and identify trends in the tectonic behavior of the sill region.

We assume that a Black Sea type of connectivity (Fig. 11.a) persisted throughout deposition of the Maikop Series creating the stratification of the water column, necessary for the maintenance of long lasting brackish anoxic environments (during the Kozakhurian stage) in the Eastern Paratethys. The next connectivity phase (Figs. 11.b, 12) is linked with

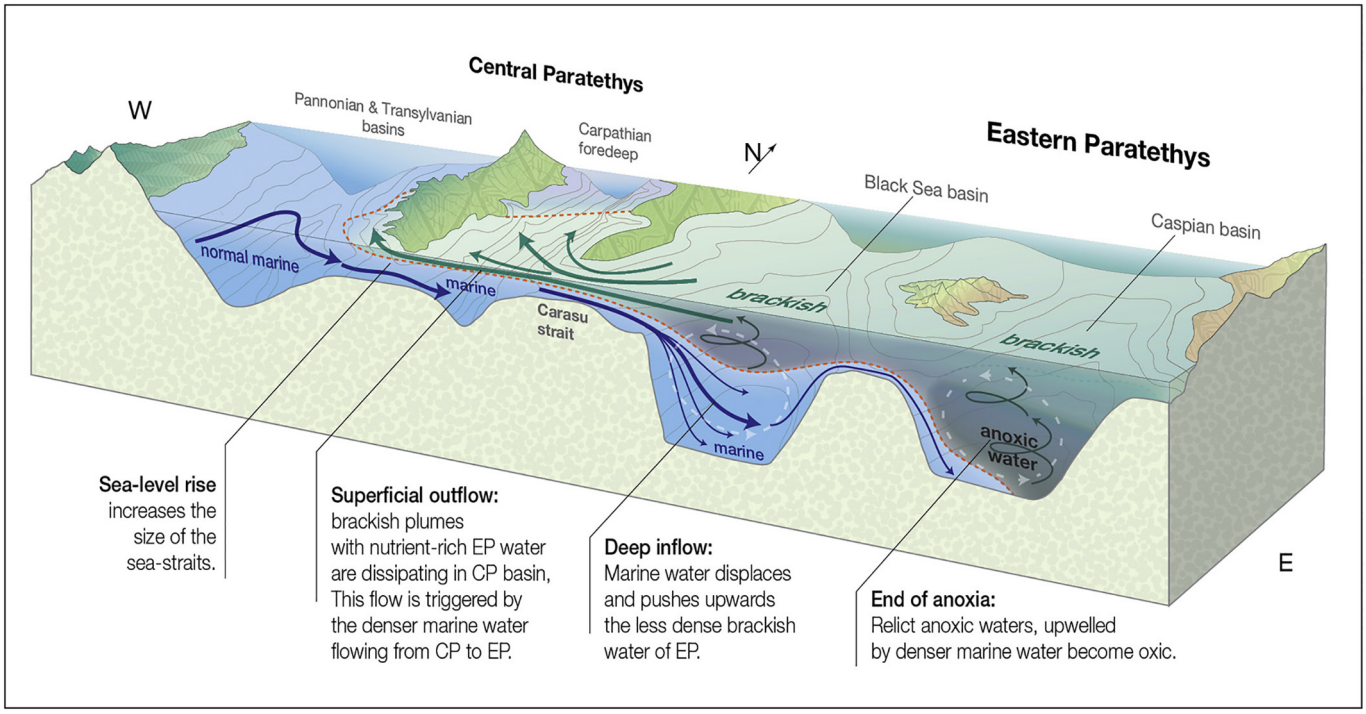

Fig. 12. The shutdown of anoxia during the Tarkhanian flooding at ~14.85 Ma. A sea-level rise triggered a short-lived phase (~100 kyr) of water exchange between Eastern Paratethys and global ocean. The sea-level rise increased the size and exchange efficiency of the Carasu strait. Denser marine water flowed in Eastern Paratethys pushing upwards and out the brackish anoxic water of the basin. This vertical circulation led to basin oxygenation.

the Tarkhanian flooding (14.85–14.75 Ma), located in the middle of a period of continuous sea level rise (+40 m between 15.2 and 14.2 Ma). After a rise of ~25 m, the threshold of water mixing is breached and open marine environments are installed in Eastern Paratethys. In this episode of peak connectivity, a massive inflow of normal marine water increases salinity, forces mixing and leads to the oxygenation of the water column (Fig. 12). This is probably the key mechanism for shutting down the long lasting Maikop anoxia in Eastern Paratethys. The sea level continued to rise throughout the lower part of the Chokrakian (14.75–14.2), in agreement with the transgressive nature of this stage. In the Chokrakian, however, open marine environments are replaced by more restricted ones, characterized by stratification and low salinity, indicating a restriction in connectivity. In the upper part of Chokrakian - beginning of the Karaganian (14.2–13.8), the sea-level dropped and connectivity was reduced, and probably even stopped (Fig. 11.c).

The new chronological framework for the end of the Maikop anoxia and the Tarkhanian flooding provides an opportunity to correlate the middle Miocene changes in gateway configuration of the Carasu Strait with the global sea level curve from the North Atlantic (Kominz et al., 2008) (Fig. 11.d).The Carasu strait is a tectonically active zone situated along the Tornquist–Teisseyre Line (Hippolyte, 2002) thus it is expected that the tectonic component will play a role too. To isolate the tectonic component, we plot a hypothetical sill curve for the Carasu strait (Fig. 11.d) in which tectonic uplift and subsidence, coupled to a lesser extent with erosion, are employed to explain the differences between the eustatic and connectivity trends.

During the Kozakhurian phase, the sea-level was low, resulting in reduced connectivity. During the following Tarkhanian phase, the Carasu Strain has been significantly enlarged by global sea level rise and/or tectonic subsidence (Fig. 11.d.1). The Tarkhanian strait geometry must have increased in size to allow a bi-directional water exchange between the basins (Fig. 11.d.2). During the early Chokrakian the connectivity decreases again, although the sea-level continues to rise. We assume that the previous bi-directional flow gets "suffocated" by tectonic uplift, which reduces connectivity (Fig. 11.d.3). As the average sea level rise slows down from the initial 10 m/kyr to 1 m/kyr (Kominz et al., 2008) tectonic uplift in the gateway regions due to the compression of the Carpathians (Tarapoanca et al., 2003, Matenco et al., 2010) probably takes over and severs the connection finally leading to isolation of the Eastern Paratethys (Fig. 11.d.4). during the Karaganian stage. We conclude that the Tarkhanian and Chokrakian stages are actually two distinct phases of a single flooding event, differentiated by changes in the functioning of the connecting gateway(s). Tectonic forcing generates transitional phases that are reflected in relatively slow connectivity changes. On the other hand, the eustatic forcing is expressed in the form of events: relatively large fluctuations that can overcome tectonics. The validity of this hypothetical sill curve for the Carasu strait, inferred by eustatic fluctuations and various degrees of connectivity, must be further evaluated with the help of structural and tectonic data from field measurements and seismic lines.

7. Conclusions

We provide integrated magneto-biostratigraphic results for two continuous, ~600 m long, sedimentary successions, situated on the southern slope of the Indol-Kuban Depression north of the Caucasus Mountains in a deep facies, with scarce fauna (Pshekha River) and a shallower facies, with more abundant fauna (Belaya River). The succession comprises the uppermost Maikopian (Kozakhurian) - Tarkhanian - Chokrakian - Karaganian - Konkian - Volhynian (lower Sarmatian s.l.) interval of the Eastern Paratethys. The magnetostratigraphic record from the Belaya section consists of fifteen different polarity intervals, seven of reverse and eight of normal polarity. The polarity pattern of the Pshekha section comprises sixteen different polarity intervals, eight of reverse and eight of normal polarity. The two sections have a common pattern that can be correlated to the GPTS. Our correlation shows that the entire succession covers the time interval from ~15 to ~12.3 Ma. We date and describe the major paleoenvironmental phases, which can all be related to changes in the configuration of the paleostraits that connected the Eastern Paratethys with the Central Paratethys and the Mediterranean due to a tectonic-eustatic interplay.

We show that the shutdown of the Paratethys anoxic giant was caused by an eastward continental scale transgression, that can be traced for >3000 km from Central Europe to Central Asia. This Tarkhanian flooding event can be correlated with chron C5Bn.1n at an age of 14.85 Ma. This marine episode was short-lived (100 kyr) in spite of the transgressive background continuing during the following Chokrakian stage. This was probably caused by tectonic uplift of the gateway area that had overcome the sea level rise.

Author contributions

Project initiated by D.P. and supervised by W.K. Sampling in the field was performed by S.P., D.P., W.K., L.G and S.L. Paleomagnetic measurements were performed D.P. (demagnetisation and rock magnetism) and SL (rock magnetism). K.K. and DP performed the Radio-isotope dating. Biostratigraphic determinations were performed by S.P. (mollusks) and L.G. (nannoplankton). Stratigraphic background was put together by S.P., L.G. and D.P with assistance from W.K. Connectivity scenarios developed by D.P. and W.K. with the help of S.P. and L.G. All authors contributed in the writing process.

Acknowledgements

Special thanks go to Roel van Elsas for his guidance. Irina Patina, Vitaly, Marina Sladkovskaya, Alexandra Rylova, Andrey Popkov, Alexander Guzhov, Pavel Frolov, Jenea Filina, Jenea and Irina Nabokovy and Kubik are thanked for their help during the fieldwork. Special thanks go also to Eleonora Radionova, Irina Goncharova and Valery Trubikhin for their support. Special thanks go to the people from Fort Hoofddijk, "the Forters" for their technical help and collegial support. The micropaleontological research complies with the state theme AAAA-A17-117030610119-6 of the Geological Institute RAS. This work in field expedition was financially supported by the Russian Foundation for Basic Research (17-05-00047 and 16-05-01032) and by the Netherlands Geosciences Foundation (ALW) with support from the Netherlands Organization for Scientific Research (NWO) through the VICI grant of WK.

References

Akhmetiev, M.A., Popov, S.V., Krhovsky, J., Goncharova, I.A., Zaporozhets, N.I., Sychevskaya, E.K., Radionova, E.P., 1995. Palaeontology and Stratigraphy of the Eocene–Miocene Sections of the Western Pre-Caucasia: Excursion Guidebook. Russian Committee for IGCP, Moscow-Krasnodar-Majkop (18 pp.).

Allen, M.B., Armstrong, H.A., 2008. Arabia–Eurasia collision and the forcing of mid-Cenozoic global cooling. Palaeogeography Palaeoclimatology Palaeoecology 265, 52–58. https://doi.org/10.1016/J.PALAEO.2008.04.021.

Andreyeva-Grigorovich, A.S., Savytskaya, N.A., 2000. Nannoplankton of the Tarkhanian deposits of the Kerch Peninsula (Crimea). Geologica Carpathica 5 (116), 399–406 (Bratislava).

Andrusov, N.I., 1884. A Note on Geological Investigations in the Vicinity of Kerch, Zap. Novorosova. Estestvoispytateley. vol. 9, no. 1 p. 15.

Andrusov, N.I., 1917. Konkian Horizon (Pholada Beds)//Proc. Geol. and Mineral. Mus. AS., V.2, ess.6. pp. 167–261 (In Russian).

Andrusov, N.I., 1918. Kerchenskiy isvestniak i ego fauna. Izbr.Trudy T.I (1961). pp. 31–112 (Moskva).

Ballato, P., Cifelli, F., Heidarzadeh, G., Ghassemi, M.R., Wickert, A.D., Hassanzadeh, J., Dupont-Nivet, G., Balling, P., Sudo, M., Zeilinger, G., Schmitt, A.K., Mattei, M., Strecker, M.R., 2017. Tectono-sedimentary evolution of the northern Iranian Plateau: insights from middle–late Miocene foreland-basin deposits. Basin Research 29, 417–446. https://doi.org/10.1111/bre.12180.

Barbot de Marny, N., 1869. Esquisse géologique du gouvernement de Cherson. Sidorenco, Les Formations Mio-pliocènique en Russie. Bull. Soc. Géol. France, Sér. III 21 (369 pp. Paris).

Barg, I.M., Ivanova, T.A., 2001. Miocene stratigraphy and geological history of the Crimean Plain Region. Stratigraphy and Geological Correlation 8 (3), 83–93.

Beluzhenko, E.V., Volkodav, I.G., Derkacheva, M.G., Korsakov, S.G., Sokolov, V.V., Chernykh, V.I., 2007. Oligocene and Neogene Sediments of the Belaya River Valley (Adygea). The Adygei state Univrsity, Maikop, p. 110.

Bobylev, V.V., Pishvanova, L.S., 1979. Predtarchanskiy pereryv v Azovo-Tschernomorskom regione i vremya zalozhenya Tschernomorskoi vpadany (The pre-Tarkhan interval in the Azov-Black Sea region and the initial stage of the Black Sea depression). Okeanologiya 19/2, 293–296 (in Russian).

Brzobohathy, R., Cicha, I., Kovac, M., Rogl, F. (Eds.), 2003. The Karpatian, a lower Miocene stage of the Central Paratethys. Masaryk University, Brno (360 pp.).

Chiriac, M., 1970. Răspîndirea şi faciesurile Tortonianului în Dobrogea de sud, Dări de seamă ale şedinţelor. 56(4). Institutul Geologic, pp. 89–112.

Cicha, I., Rogl, F., Rupp, Ch., Ctyroka, J. (Eds.), 1998. Oligocene-Miocene foraminifera of the Central Paratethys. Abh. senkenberg. naturforsch. Ges 549 (325 pp., 79 pl., Frankfurt a. M.).

Davitashvili, L.Sh, 1933. Most important fossils of Crimea Caucasus oil area. V.2: Tarkhanian and Chokrakian Horizons. Tr. State Res. Oil Inst, Moscow, p. 1168 (in Russian).

De Leeuw, A., Bukowski, K., Krijgsman, W., Kuiper, K.F., 2010. Age of the Badenian salinity crisis; impact of Miocene climate variability on the circum-Mediterranean region. Geology 38 (8), 715–718.

De Leeuw, A., Filipescu, S., Maţenco, L., Krijgsman, W., Kuiper, K., Stoica, M., 2013. Paleomagnetic and chronostratigraphic constraints on the middle to late Miocene evolution of the Transylvanian basin (Romania): implications for Central Paratethys stratigraphy and emplacement of the Tisza-Dacia plate. Global and Planetary Change 103 (1), 82–98.

Dekkers, M.J., Passier, H.F., Schoonen, M.A.A., 2000. Magnetic properties of hydrothermally synthesized greigite (Fe_3S_4) II. High- and low-temperature characteristics. Geophysical Journal International 141, 809–819.

Gavrilov, Y.O., 2017. Reflection of seismic paleoevents in MesozoiceCenozoic terrigenous sequences of the Northern Caucasus. Lithology and Mineral Resources 52, 1–19.

Golovina, L.A., 2012. On the question of stratigraphy of the Middle–Upper Miocene of southern Russia based on calcareous nannoplankton. 15th AllRussia Micropaleontological Conference on Modern Micropaleontology, pp. 305–308 (Gelendzhik).

Golovina, L., Goncharova, I., Rostovtseva, Yu., 2004. New data on biostratigraphy (nannoplankton, molluscs) and lithology of the Middle Miocene of Taman Peninsula and the Western Caucasus. Stratigraphy and Geological Correlation 12 (6), 103–112.

Golovina, L.A., Vernigorova, Yu.V., Beluzhenko, E.V., 2009. New Data About Micropaleontology From the Konkian Deposits of the Western Ciscaucasia. Proceedings of the Institute of Geological Sciences of the NAS of Ukraine, Kyiv, pp. 311–321.

Goncharova, I.A., 1989. Dvustvorchatyie molluski tarkhanskogo i chokrakskogo basseynov [Bivalve molluscs of the Tarkhanian and Chokrakian basins]. Trudy Paleontologičeskogo Instituta, Akademiya Nauk SSR 234, 200.

Goncharova, L.A., Il'ina, L.B., 1997. Relations between Middle Miocene Basin of the Western and Eastern Paratethys. Stratigraphy and Geological Correlation 5 (6), 74–82.

Goncharova, I.A., Khondkarian, S.O., Shcherba, I.G., 2001. The Tarkhanian-Karaganian stage in development of the Euxinian-Caspian Basin (Eastern Paratethys), part 1: Tarkhanian. Stratigraphy and Geological Correlation 9 (5), 508–522.

Guzhov, A., 2017. New data about geographical distribution of the Early Chokrakian gastropods [In Russian]. Proceedings of the All-Russian Scientific Practical Conference "Geology and biodiversity of the Tethys and Eastern Paratethys", Goryachy Klyuch, pp. 24–30.

Harrison, R.J., Feinberg, J.M., 2008. FORCinel: an improved algorithm for calculating first-order reversal curve distributions using locally weighted regression smoothing. Geochemistry, Geophysics, Geosystems 9, Q05016. https://doi.org/10.1029/2008GC001987.

Harzhauser, M., Piller, W., Steininger, F.F., 2002. Circum-Mediterranean Oligo-Miocene biogeographic evolution - the gastropods' point of view. Palaeogeography, Palaeoclimatology, Palaeoecology 183 (2002), 103–133. https://doi.org/10.1016/S0031-0182(01)00464-3.

Hilgen, F.J., Lourens, L.J., Van Dam, J.A., Beu, A.G., Boyes, A.F., Cooper, R.A., Krijgsman, W., Ogg, J.G., Piller, W.E., Wilson, D.S., 2012. The Neogene Period. The Geologic Time Scale 2012 1–2 pp. 923–978.

Hippolyte, J.-C., 2002. Geodynamics of Dobrogea (Romania): new constraints on the evolution of the Tornquist–Teisseyre Line, the Black Sea and the Carpathians. Tectonophysics 357, 33–53.

Hüsing, S.K., Zachariasse, W.-J., Van Hinsbergen, D.J.J., 2009. Oligocenee Miocene basin evolution in SE Anatolia, Turkey: constraints on the closure of the central Tethys gateway. In: Van Hinsbergen, D.J.J., Edwards, M.A., Govers, R. (Eds.), Collision and Collapse at the Africa-Arabia-Eurasia Subduction Zone. Geological Society, London, Special Publications vol. 311, pp. 107–132.

Iljina, L.B., 1995. Connections of Eastern Paratethys paleobasins with Tethyan seas in middle and late Miocene. Abstracts10th Congress RCMNS. Romanian Journal of Stratigraphy 76 (suppl. nr. 7), 157.

Ivanova, T.A., 1999. Biostratigraphy of the Miocene Deposits in Crimean Lowlands by Foraminifera. (PhD thesis). 16. Publ. Inst. Geol. NAN Ukraine.

Jones, R.W., Simmons, M.D., 1996. A review of the stratigraphy of Eastern Paratethys (Oligocene–Miocene). Bulletin of the Natural History Museum 52, 25–49.

Katz, B., Richards, D., Long, D., Lawrence, W., 2000. A new look at the components of the petroleum system of the South Caspian Basin. Journal of Petroleum Science and Engineering 28, 161–182.

Kelder, N.A., Sant, K., Dekkers, M.J., Magyar, I., Van Dijk, G.A., Lathouwers, Y.Z., Sztanó, O., Krijgsman, W., 2018. Paleomagnetism in Lake Pannon; problems, pitfalls and progress in using iron sulfides for magnetostratigraphy. Geochemistry, Geophysics, Geosystems https://doi.org/10.1029/2018GC007673 (in press).

Kirschvink, J.L., 1980. The least-squares line and plane and the analysis of palaeomagnetic data. Geophysical Journal of the Royal Astronomical Society 62 (3), 699–718.

Kokay, J., 1985. Central and Eastern Paratethyan interrelations in the light of Late Badenian salinity conditions. Geologica Hungarica, Series Palaeontologica, Fasciculus 48, pp. 7–96.

Kominz, M.A., Browning, J.V., Miller, K.G., Sugarman, P.J., Mizintseva, S., Scotese, C.R., 2008. Late Cretaceous to Miocene sea-level estimates from the New Jersey and Delaware coastal plain boreholes: an error analysis. Basin Research 20, 211–226. https://doi.org/10.1111/j.1365-2117.2008.00354.x.

Konenkova, I.D., Bogdanovich, E.I., 1994. Distribution pattern of foraminifera and nannoplankton within the Tarkhanian-Tschokrakian deposits of the Malij Kamyshlak

section (Kerch Peninsula). In: Teslenko, Y.V. (Ed.)Ancient Biospheres of the Ukraine 1. National Academy of Sciences of the Ukraine, Kiev, pp. 95–96 (In Russian).
Koppers, A.A.P., 2002. ArArCALC-software for40Ar/39Ar age calculations. Computers and Geosciences 28, 605–619. https://doi.org/10.1016/S0098-3004(01)00095-4.
Kováč, M., Andreyeva-Grigorovich, A., Bajraktarević, Z., Brzobohatý, R., Filipescu, S., Fodor, L., Harzhauser, M., Nagymarosy, A., Oszczypko, N., Pavelić, D., Rögl, F., Saftić, B., Sliva, L., Studencka, B., 2007. Badenian evolution of the Central Paratethys Sea: paleogeography, climate and eustatic sea-level changes. Geologica Carpathica 58 (6), 579–606.
Kováč, M., Halásová, E.V.A., Hudáčková, N., Holcová, K., Hyžný, M., Jamrich, M., Ruman, A., 2018. Towards better correlation of the Central Paratethys regional time scale with the standard geological time scale of the Miocene Epoch. , pp. 283–300 https://doi.org/10.1515/geoca-2018-0017.
Krasheninnikov, V.A., Basov, I.A., Golovina, L.A., 2003. The Eastern Paratethys: Tarkhanian and Konkian Regional Stages. Nauchn. Mir. P, Moscow.
Krijgsman, W., Stoica, M., Vasiliev, I., Popov, V.V., 2010. Rise and fall of the Paratethys Sea during the Messinian Salinity Crisis. Earth and Planetary Science Letters 290 (1–2), 183–191.
Kuiper, K.F., Deino, A., Hilgen, F.J., Krijgsman, W., Renne, P.R., Wijbrans, J.R., 2008. Synchronizing rock clocks of earth history. Science 320, 500–504. https://doi.org/10.1126/science.1154339 (80-.).
Langereis, C.G., Krijgsman, W., Muttoni, G., Menning, M., 2010. Magnetostratigraphy – concepts, definitions, and applications. Newsletters on Stratigraphy 43, 207–233.
Laskarev, V., 1924. Sur les équivalents du Sarmatien supérieur en Serbie. Recueil de traveaux offert à M. Jovan Cvijic par ses amis et collaborateurs, pp. 73–85.
Lee, J.Y., Marti, K., Severinghaus, J.P., Kawamura, K., Yoo, H.S., Lee, J.B., Kim, J.S., 2006. A redetermination of the isotopic abundances of atmospheric Ar. Geochimica et Cosmochimica Acta 70, 4507–4512. https://doi.org/10.1016/j.gca.2006.06.1563.
Liu, S., Krijgsman, W., Dekkers, M.J., Palcu, D., 2017. Early diagenetic greigite as an indicator of paleosalinity changes in the middle Miocene Paratethys Sea of central Europe. Geochemistry, Geophysics, Geosystems 18, 2634–2645. https://doi.org/10.1002/2017GC006988.
Matenco, L., Krézsek, C., Merten, S., Schmid, S., Cloetingh, S., Andriessen, P., 2010. Characteristics of collisional orogens with low topographic build-up: An example from the Carpathians. Terra Nova https://doi.org/10.1111/j.1365-3121.2010.00931.x.
Min, K., Mundil, R., Renne, P.R., Ludwig, K.R., 2000. A test for systematic errors in40Ar/39Ar geochronology through comparison with U/Pb analysis of a 1.1-Ga rhyolite. Geochimica et Cosmochimica Acta 64, 73–98. https://doi.org/10.1016/S0016-7037(99)00204-5.
Mullender, T.A.T., van Velzen, A.J., Dekkers, M.J., 1993. Continuous drift correction and separate identification of ferrimagnetic and paramagnetic contributions in thermomagnetic runs. Geophysical Journal International 114, 663–672.
Mullender, T.A.T., Frederichs, T., Hilgenfeldt, C., De Groot, L.V., Fabian, K., Dekkers, M.J., 2016. Automated paleomagnetic and rock magnetic data acquisition with an in-line horizontal '2G' system. Geochemistry, Geophysics, Geosystems 17, 3546–3559.
Nevesskaya, L.A., Goncharova, I.A., Ilyina, L.B., Paramonova, N.P., Popov, S.V., Bogdanovich, A.K., Gabunia, L.K., Nosovskii, M.F., 1984. The regional stratigraphic scale of the Neogene of the Eastern Paratethys. Sovetskaya Geologiya 9, 37–49 (in Russian).
Nevesskaya, L.A., Goncharova, I.A., Ilyina, L.B., Paramonova, N.P., Popov, S.V., Babak, E.V., Bagdasarian, K.G., Voronina, A.A., 1986. The History of the Neogene Paratethys Mollusk (Nauka). 220. Paleontological Institute of the USSR Academy of Sciences (208 pp.).
Nevesskaya, L., Goncharova, I.A., Ilyina, L., Paramonova, N., Khondkarian, S.O., 2003. The Neogene stratigraphic scale of the Eastern Paratethys. Stratigraphy and Geological Correlation 11 (2), 105–127.
Nevesskaya, L.A., Kovalenko, E.I., Beluzhenko, E.V., et al., 2005a. Regional Stratigraphic Scheme of the Neogene of Southern European Part of Russia//Stratigrafiya, Regionalnaya Geologiya i Tektonika. 4 pp. 47–59 (in Russian).
Nevesskaya, L., Goncharova, I.A., Ilyina, L., 2005b. Types of Neogene marine and nonmarine basins exemplified by the Eastern Paratethys. Paleontological Journal 39 (3), 227–235.
Palcu, D., Tulbure, M., Bartol, M., Kouwenhoven, T.J., Krijgsman, W., 2015. The Badenian–Sarmatian extinction event in the Carpathian foredeep basin of Romania: paleogeographic changes in the Paratethys domain. Global and Planetary Change 133, 346–358.
Palcu, D.V., Golovina, L.A., Vernyhorova, Y.V., Popov, S.V., Krijgsman, W., 2017. Middle Miocene paleoenvironmental crises in Central Eurasia caused by changes in marine gateway configuration. Global and Planetary Change 158, 57–71. https://doi.org/10.1016/j.gloplacha.2017.09.013.
Palcu, D.V., Vasiliev, I., Stoica, M., Krijgsman, W., 2018. The end of the Great Khersonian Drying of Eurasia: magnetostratigraphic dating of the Maeotian transgression in the Eastern Paratethys. Basin Research https://doi.org/10.1111/bre.12307.
Paleontology and stratigraphy of the Middle–Upper Miocene of Taman Peninsula. Part 1. Description of key-sections and benthic fossil groups. In: Popov, S.V., Golovina, L.A. (Eds.), Paleontol. Journ. Suppl. Ser. vol. 50, no. 10 (168 pp.).
Passier, H.F., de Lange, G.J., Dekkers, M.J., 2001. Rock-magnetic properties and geochemistry of the active oxidation front and the youngest sapropel in the Mediterranean. Geophysical Journal International 145, 604–614.
Paulissen, W., Luthi, S., Grunert, P., Čorić, S., Harzhauser, M., 2011. Integrated high-resolution stratigraphy of a Middle to Late Miocene sedimentary sequence in the central part of the Vienna Basin. Geologica Carpathica 62 (2), 155–169.
Peryt, T.M., Peryt, D., Jasionowski, M., Poberezhskyy, A.V., Durakiewicz, T., 2004. Post-evaporitic restricted deposition in the Middle Miocene Chokrakian-Karaganian of East Crimea (Ukraine). Sedimentary Geology 170 (1–2), 21–36.
Phillips, D., Matchan, E.L., 2013. Ultra-high precision40Ar/39Ar ages for Fish Canyon Tuff and Alder Creek Rhyolite sanidine: New dating standards required? Geochimica et Cosmochimica Acta 121, 229–239. https://doi.org/10.1016/j.gca.2013.07.003.
Piller, W.E., Harzhauser, M., Mandic, O., 2007. Miocene Central Paratethys stratigraphy — current status and future directions. Stratigraphy 4, 151–168.
Poisson, A., Vrielynck, B., Wernli, R., et al., 2016. Miocene transgression in the central and eastern parts of the Sivas Basin (Central Anatolia, Turkey) and the Cenozoic palaeogeographical evolution. International Journal of Earth Sciences (Geologische Rundschau) 105, 339. https://doi.org/10.1007/s00531-015-1248-1.
Popkhadze, L., 2016. Palaeoecological Issues of Tarkhanian-Chokrakian Basins of Western Georgia according to Microfauna (Foraminifers, Ostracodes). Bulletin of the Georgian National Academy of Sciences 10 (4), 2016.
Popov, S.V., Voronina, A.A., 1983. The Kotsakhurian Phase in the Development of the Eastern Paratethys. Izvestiya Akademii Nauk SSSR. Seriya Geologicheskaya No. 1, 58–67 [in Russian].
Popov, S.V, Voronina, A.A., Goncharova, L.A., 1993. Stratigraphy and Bivalves of the Oligocene-Lower Miocene of the Eastern Paratethys (Nauka, Moscow, 1993) [in Russian].
Popov, S.V., Shcherba, I.G., Khondkarian, S.O., Ilyina, L.B., Paramonova, N.P., Khondkarian, S.O., et al., 2004. Lithological-Paleogeographic Maps of Paratethys. 250. Courer Forschungsinstitut Senckenberg Frankfurt a. M, pp. 1–46 (10 maps).
Popov, S.V., Shcherba, I.G., Ilyina, L.B., Nevesskaya, L.A., Paramonova, N.P., Khondkarian, S.O., Magyar, I., 2006. Late Miocene to Pliocene palaeogeography of the Paratethys and its relation to the Mediterranean. Palaeogeography, Palaeoclimatology, Palaeoecology 238 (1–4), 91–106.
Popov, S.V., Golovina, L.A., Jafarzadeh, M., Goncharova, I.A., 2015. Eastern Paratethys Miocene Deposits, Mollusks and Nannoplankton of the Northern Iran//Neogene of the Paratethyan Region, 6 Workshop on Neogene of Central and SE Europe, 31 May–3 June 2015, Orfu, Hungary. pp. 71–72.
ter Borgh, M., Vasiliev, I., Stoica, M., Knežević, S., Matenco, L., Krijgsman, W., Rundić, L., Cloetingh, S., 2013. The isolation of the Pannonian basin (Central Paratethys): new constraints from magnetostratigraphy and biostratigraphy. Global and Planetary Change 103 (1), 99–118.
Radionova, E.P., Golovina, L.A., 2012. Upper Maeotian Lower Pontian "Transitional Strata" in the Taman Peninsula: stratigraphic position and paleogeographic interpretation. Geologica Carpathica 62 (1), 62–100.
Reuter, M., Piller, W.E., Harzhauser, M., Mandic, O., Berning, B., Rögl, F., Kroh, A., Aubry, M.P., Wielandt-Schuster, U., Hamedani, A., 2009. The Oligo-/Miocene Qom formation (Iran): Evidence for an early Burdigalian restriction of the Tethyan Seaway and closure of its Iranian gateways. International Journal of Earth Sciences 98, 627–650. https://doi.org/10.1007/s00531-007-0269-9.
Roberts, A.P., Liu, Q.S., Rowan, C.J., Chang, L., Carvallo, C., Torrent, J., Horng, C.S., 2006. Characterization of hematite (Fe_2O_3), goethite (FeOOH), greigite (Fe_3S_4), and pyrrhotite (Fe_7S_8) using first-order reversal curve diagrams. Journal of Geophysical Research 111, B12S35.
Roberts, A.P., Chang, L., Rowan, C.J., Horng, C.S., Florindo, F., 2011. Magnetic properties of sedimentary greigite (Fe_3S_4): an update. Reviews of Geophysics 49, RG1002.
Robinson, A.G., Rudat, J.H., Banks, C.J., Wiles, R.L.F., 1996. Petroleum geology of the Black Sea. Marine and Petroleum Geology 13, 195–223.
Rögl, F., 1998. Palaeogeographic considerations for Mediterranean and Paratethys seaways (Oligocene to Miocene). Annalen des Naturhistorischen Museums Wien 99A (A), 279–310.
Rögl, F., Muller, C., 1976. Das Mittelmiozan und die Baden – Sarmat Grenze im Walbersdorf (Burgenland). Annalen des Naturhistorischen Museums Wien 80, 221–232 (Wien).
Ruban, D.A., Rogerson, M., Pedley, H.M., 2010. Do major Neogene hiatuses in the Ciscaucasian semi-enclosed basin (Eastern Paratethys, southwestern Russia) record eustatic falls? Geoloski Anali Balkaanskoga Poluostrva https://doi.org/10.2298/GABP1071001R.
Sachsenhofer, R.F., Popov, S.V., Bechtel, A., Coric, S., Francu, J., Gratzer, R., Grunert, P., Kotarba, M., Mayer, J., Pupp, M., Rupprecht, B.J., Vincent, S.J., 2017. Oligocene and Lower Miocene source rocks in the Paratethys: palaeogeographical and stratigraphic controls. Geological Society, London, Special Publications 464, 7 September 2017. https://doi.org/10.1144/SP464.1.
Sant, K., Palcu, D.V., Mandic, O., Krijgsman, W., 2017. Changing seas in the Early-Middle Miocene of Central Europe. Terra Nova https://doi.org/10.1111/ter.12273.
Sant, K., Palcu, D.V., Turco, E., Di Stefano, A., Baldassini, N., Kouwenhoven, T., Kuiper, K.F., Krijgsman, W., 2018. The mid-Langhian flooding in the eastern Central Paratethys: integrated stratigraphic data from the Transylvanian Basin and SE Carpathian Foredeep. IJES (submitted).
Schultz, H.M., Bechtel, A., Sachsenhofer, R.F., 2005. The birth of Paratethys during the early Oligocene: from Tethys to an ancient Black Sea Analogue? Global and Planetary Change 49, 163–176.
Steininger, F.F., Rogl, F., Muller, C., 1978. Geodynamik und palaeogeographische Entwicklung des Badenien. In: Papp, A., Cicha, I., Senes, J., Steininger, F.F. (Eds.), Chronostratigraphie und Neostratotypen. Miozan der Zentralen Paratethys, 6: Badenian. Veda, Bratislava, pp. 110–127.
Tarapoanca, M., Bertotti, G., Matenco, L., Dinu, C., Cloetingh, S., 2003. Architecture of the Focsani Depression: A 13 km deep basin in the Carpathians bend zone (Romania) 22. https://doi.org/10.1029/2002TC001486.
Van Baak, C.G.C., Vasiliev, I., Palcu, D.V., Dekkers, M.J., Krijgsman, W., 2016. A greigite-based magnetostratigraphic time frame for the Late Miocene to Recent DSDP Leg 42B cores from the Black Sea. Frontiers in Earth Science 4 (60). https://doi.org/10.3389/feart.2016.00060.
Van der Boon, A., Kuiper, K.F., Villa, G., Renema, W., Meijers, M.J.M., Langereis, C.G., Aliyeva, E., Krijgsman, W., 2017. Onset of Maikop sedimentation and cessation of Eocene arc volcanism in the Talysh Mountains, Azerbaijan. In: Sosson, M., Stephenson, R.A., Adamia, S.A. (Eds.), Tectonic Evolution of the Eastern Black Sea and Caucasus. Geol. Soc. London, Spec. Publ 428. https://doi.org/10.1144/SP428.3.

Van der Boon, A., Beniest, A., Ciurej, A., Gazdzicka, E., Grothe, A., Sachsenhofer, R., Langereis, C.G., Krijgsman, W., 2018. The Eocene-Oligocene transition in the North Alpine Foreland Basin and subsequent closure of a Paratethys gateway. Global and Planetary Change https://doi.org/10.1016/j.gloplacha.2017.12.009.

Vangengeim, E.A., Tesakov, A.S., 2008. Maeotian mammalian localities of Eastern Paratethys: magnetochronology and position in European continental scales. Stratigraphy and Geological Correlation 16 (4), 95–109. https://doi.org/10.1134/S0869593808040060.

Vangengeim, E.A., Lungu, A.N., Tesakov, A.S., 2006. Age of the Vallesian Lower Boundary (Continental Miocene of Europe). Stratigraphy and Geological Correlation 14 (6), 655–667. https://doi.org/10.1134/S0869593806060050.

Vasiliev, I., et al., 2008. Putative greigite magnetofossils from the Pliocene epoch. Nature Geoscience (11), 782–786.

Vasiliev, I., de Leeuw, A., Filipescu, S., Krijgsman, W., Kuiper, K., Stoica, M., Briceag, A., 2010. The age of the Sarmatian-Pannonian transition in the Transylvanian Basin (Central Paratethys). Palaeogeography, Palaeoclimatology, Palaeoecology 297 (1), 54–69.

Vasiliev, I., Iosifidi, A.G., Khramov, A.N., Krijgsman, W., Kuiper, K., Langereis, C.G., Popov, V.V., Stoica, M., Tomsha, V.A., Yudin, S.V., 2011. Magnetostratigraphy and radioisotope dating of upper Miocene-lower Pliocene sedimentary successions of the Black Sea Basin (Taman Peninsula, Russia). Palaeogeography, Palaeoclimatology, Palaeoecology 310 (3–4), 163–175.

Zijderveld, J.D.A., 1967. AC demagnetization of rocks: analysis of results. Methods in Paleomagnetism, pp. 254–286.